Robotica (2018) volume 36, pp. 1111–1143. © Cambridge University Press 2018
doi:10.1017/S0263574718000267

Kinematic and dynamic performance investigations of asymmetric (U-shape fixed base) planar parallel manipulators

Jayant Kumar Mohanta†, Yogesh Singh‡, and Santhakumar Mohan†,*

†*Mechanical Engineering, Indian Institute of Technology Indore, Indore 453552, India.*
E-mail: jkmjayant@gmail.com
‡*Mechanical Engineering, SRM Institute of Science and Technology, Chennai 603203, India.*
E-mail: yogeshsingh15@gmail.com

(Accepted March 10, 2018. First published online: April 6, 2018)

SUMMARY
In this paper, a new family of 3-degree-of-freedom planar parallel manipulators (PPMs), namely U-shape fixed base PPMs starting with an active prismatic joint on each leg, is proposed. In order to identify the best manipulators of this family, comparative kinematic and dynamic performance studies are performed. The kinematic performances are quantified through the local performance index, namely the kinematic isotropy. From the kinematic isotropy analysis results, it is observed that PPR-PRP-PRP, PRP-PRP-PRP and PRR-PRP-PRP configurations have better kinematic design aspects compared to other configurations of this family of U-shape fixed base parallel configurations. Further, from the workspace analysis, it is observed that the PPR-PRP-PRP configuration has a higher value of workspace to the total area required ratio compared to other configurations. This paper also presents a comparative dynamic performance analysis of these top-three U-shape fixed base configurations in terms of dynamic driving performance measures, and energy requirements for three different (fixed base size of the manipulators) aspect ratios under two different loading conditions. From the analyses results, it is perceived that the PRP-PRP-PRP configuration is requiring lower energy and dynamic driving performances than others. These analyses are done with the help of multi-body dynamic software, namely MSC ADAMS, and the results are validated through the help of real-time experiments conducted on in-house fabricated prototypes of these three PPMs. In specific, the energy consumption is measured and compared in this study. Experimental results demonstrated that the PRP-PRP-PRP manipulator displays a considerably better performance in terms of minimum energy requirement.

KEYWORDS: Planar parallel manipulator, Kinematic analysis, Dynamic analysis, Kinematic isotropy, Dynamic performance measures

ABBREVIATIONS: R, Rotary/revolute joint; P, Prismatic/translation joint; P, powered/active prismatic joint

1. Introduction

1.1. Planar parallel manipulators

Planar parallel manipulators (PPMs) and parallel kinematic mechanisms have been comprehensively studied by many researchers because of their potential advantages over serial manipulators,[1] namely high speed, more accurate, better precision, lower inertia of the moving parts and they do not suffer from error accumulation issues. Most of the researchers have focused their work on the spatial parallel

* Corresponding author. E-mail: santhakumar@iiti.ac.in

manipulators, but the applications of the PPMs are numerous and hence necessitating a proper analysis for the efficient design.[2–4] The PPMs have their motions restricted to a plane with the usage of prismatic and revolute joints. The moving platform (end-effector) of a PPM is linked or connected to a fixed platform using at least three kinematic chains (legs), where each leg is having at least three single degrees-of-freedom (DOF) joints in which one of the joints is an active prismatic/revolute joint, which is usually connected to the fixed platform. Placement of actuators in the fixed platform (base) allows the end-effector to reach higher speed and acceleration.[1–4] These motion platforms/manipulators have a wider range of applications such as material handling and processing, fabrication, micro-machining and precise positioning devices because of simplicity in their joint arrangements (kinematic configurations) and their movements can be restricted in a plane. A number of configurations have been proposed by varying the kinematic configuration of the 3-DOF kinematic chain/leg, namely 3-RRR, 3-PRR, 3-PPR, 3-PRP, 3-RRP, 3-RPP and combinations of the kinematic arrangements in these legs (PRP+PPR+RRR, PRP+PRP+PPR, etc.) in the past, and the success rates of the configurations depend on their applications.[1–25] The kinematics and design of PPMs have been extensively studied.[1] Merlet[2] focused on the direct kinematic problem associated with particular architectures of PPMs, namely 3-RPP, 3-RRP, 3-RRR, 3-RPR, 3PPR, 3PRP and 3PRR. Different type of workspace for these manipulators were analysed such as dexterous, reachable and orientation workspace. Joubair[3] presented a new partially decoupled 3-DOF (2-PRP and 1-PPR) planar parallel mechanism that can deliver accurate positioning and has a higher workspace compared to the other existing 3-DOF PPMs. The first limb of this manipulator is associated with the PPR (prismatic-prismatic-revolute) and placed along the x-axis. The remaining two limbs of the manipulator are associated with the PRP (prismatic-revolute-prismatic) and placed along the y-axis. The manipulator has the larger base (fixed platform) compared to its workspace and has a limitation in terms of orientation angle. Choi[6] proposed a 3-DOF 3-PPR PPM in association with one active prismatic joint in each limb out of three kinematic limbs. The proposed 3-PPR PPM has the advantages of the closed-type direct kinematics and singular-free workspace, but the manipulator has the limitation in terms of speed and structural stiffness. Rezaei and Akbarzadeh[10] proposed a new 3-DOF 2-PRR-1-PPR axis asymmetric PPM,, and it is observed that the manipulator has lower workspace as well as fully coupled kinematic solutions that will affect the overall performance of the system. Gogu[11–14] revealed the possibilities of design of PPMs with three limbs. Due to its huge number of joints and lower load-carrying capacity of the end-effector, the configurations revealed are not suitable for the precise positioning devices. Yu[15] discussed a simple geometric approach to analyse the position and orientation error for a 3-DOF fully PPM. The author discussed about the three-different PPMs (namely 3-PRP (Hephaist Seiko), 2-PRP-1-PPR (PreXYT) and 3-PPR (star triangle mechanism)) and presented their accuracy. It is found from the analyses that the 2-PRP-1-PPR planar parallel mechanism has partially decoupled kinematic solution, larger singular-free workspace with smaller values of mechanical errors and lower workspace to size ratio due to their fixed base shape. Bonev[4,17] presented a 3-DOF planar parallel mechanism (PreXYT), which is partially decoupled, rigid in all directions and has a relatively large workspace, with guide ways provided for X and Y movements, and proposed a geometric procedure for the kinematic calibration of the manipulator. Briot and Bonev[17] proposed a simpler method based on a detailed error analysis of a 3-DOF PPM that brings valuable understanding to the problem of error amplification. 3-RPR PPM is used for this error and accuracy analysis. Staicu[18,24] introduced a recursive method to reduce the number of equations and computations required, considerably by using a set of matrices for kinematics and dynamics models of the 3-PRR planar parallel robot. But, this manipulator has a limited workspace and restricts its overall positioning capabilities due to its structural arrangements. Bai and Caro[7,19,20] proposed a planar 3-PPR parallel robot with a non-symmetrical base. The topology of base platform design is addressed to maximise the manipulator's workspace. This work proposed a U-shape base manipulator along with its structural design and analysed its performance. It reveals some interesting features, such as decoupled 3-DOF and large reachable and orientation workspace but having the less workspace to base size ratio. Wu[21,23] presented a kinematic and dynamic performance comparison study of three planar 3-DOF parallel manipulators with different architectures, namely 4-RRR, 3-RRR and 2-RRR. It is found from the performance analysis that the 4-RRR PPM is better in terms of design aspects than other manipulators. Wu[22] established an error prediction model that dealt with the error modelling and analysis of a new 3-PPR PPM with joint clearances. Cartesian workspace of the 3-PPR PPMs analysed and revealed that the proposed manipulator has higher workspace.

https://doi.org/10.1017/S0263574718000267 Published online by Cambridge University Press

It is observed from the prior research on different PPMs that the design and development of different architectures of 3-DOF PPMs in association with the kinematic analysis are based on the symmetric topology[10,11,14,16,18,23] (equilateral triangle base), which implies that all three limbs are equally spaced and have a few limitations as discussed above. To overcome the limitations, a new family of the PPM is investigated in the present paper whose fixed base is in the shape of U. The present work is motivated from the previous research on U-shape fixed base PPMs, namely 3-PPR U base, 3-PRP (Hephaist), 2-PRR-1-PPR and PreXYT.[3,4,6,15,17]

1.2. Kinematic and dynamic performance measures

Kinematic and dynamic performance measures or quantifiers are the important tools to describe the manipulator performance. Kinematic aspects of the manipulators are relatively simple compared to the dynamic design aspects, as the latter work with a detailed description of the mechanism structure and their evaluation is a time-consuming and tedious process as well. The kinematic performance measures concern about the quality of the workspace, dexterity, manipulation ability, payload capacity, etc., which consider the manipulators' shape, size and presence of singularities in their design. However, the kinematic performance measures of the manipulators are dependent on their kinematic arrangements, but the dynamic performance measures are not only depending on kinematic arrangements but also on their inertial characteristics.[26,27] Manipulator dynamics is an important tool to understand the different design perspective of manipulators (parallel and serial).[11–13,28–32] It is very difficult to predict the force/torque requirements of actuators and hard to select the size and proper actuators without realising the behaviour of the system or understanding the nature of the system. Although several dynamic performance indices have been investigated in the literature,[29,30–32] the dynamic driving performance measure is one of the important tools to evaluate the manipulator performance characteristics. The dynamic performance measure is a performance index, which evaluates the force/torque margin of the joint forces/torques of the manipulator with the consideration of the masses of links, joints, moving and base platform (the dynamic part of the system, such as mass matrix, Coriolis, centripetal and gravitational effects). It reveals the energy and actuator input requirements of the manipulator. The driving performance of the manipulator becomes better as the dynamic performance index becomes smaller.[8,21,23,30,36] The dynamic performance measures of the manipulators are related to the moving masses, dynamic dexterity and the dynamically moving capability of the manipulators. A few investigations on the dynamic driving performance measures of the PPMs are performed and reported in the literature.[21,24,30–34] Extensive research studies have been done in the field of kinematic and dynamic performance aspects of the identical kinematic chain and symmetrical shape PPMs, namely 3RRR, 3RPR, 3RPP, 3RRP, 3PRR, 3PPR and 3PRR.[15–25] Similarly, a few researchers[30–42] reveal the information related to the manipulator speed, quality of workspace and capacity of the actuators. In addition, the energy requirements of the manipulator during the desired motion are providing suitable information for the selection of actuators, efficiency and cost of the system.

1.3. Contribution

The detailed performance analyses of the possible U-shape fixed base PPMs and their performance comparison studies in terms of design aspects are required to reveal or identify the best manipulators out of all the possible manipulators. Therefore, this present paper proposes the following:

- A comparative kinematic performance analysis of these possible unique manipulators is performed to identify the best possible manipulators through the help of kinematic isotropy.
- From the comparative kinematic isotropy analysis, top-three kinematic configurations are identified and considered for the further study.
- A comparative dynamic performance study of these top-three U-shape fixed base PPMs is investigated and analysed through the help of simulations in MSC ADAMS and verified using the in-house fabricated prototype experiments.

The rest of the paper is organised in the following manner: Section 2 describes the identification of the best possible PPMs based on the kinematic isotropy and workspace to total space required ratio. Section 3 discusses the dynamic performance measures and energy requirements for the top-three manipulators in a comparative manner. In Section 4, energy requirements of the top-three manipulators

https://doi.org/10.1017/S0263574718000267 Published online by Cambridge University Press

are analysed through the help of real-time experiments performed on the in-house fabricated prototypes and their numerical results are validated. Finally, in Section 5, concluding remarks are presented.

2. U-Shape Fixed Base Planar Parallel Manipulators

The 3-DOF PPMs usually have three legs and each leg has 3-DOF due to its link and joint arrangements.[1–25] In this respect, only eight kinematic configurations/legs (link and joint arrangements) are possible, namely RRR, PRP, RPR, PRR, PPR, RPP, RRP and PPP. Out of these kinematic configurations, the PPP configuration is ignored due to the fact that it does not allow any rotation to the end-effector (mobile platform) of the manipulator. Therefore, only seven configurations are possible for developing the PPMs and any of these configurations can be used as a leg of the manipulator. Thus, as per the repetition theory of permutation and combination, it achieves m^n possible combinations, where m is the number of configurations and n is the number of legs; by substituting this theory, it produces $7^3 = 343$ possible kinematic arrangements, and in other words it gives 343 PPMs. However, using a prismatic joint as a first joint of each leg gives further advantages in terms of back drivability, compactness, modular design, large singularity-free workspace, reduction in the link interferences, ease of control, simple kinematic arrangement and low inertial properties of the moving system.[1–4,15] Furthermore, using a ball/lead screw pair as an active prismatic joint has an advantage in terms of high mechanical advantage. As a result, many industrial manipulators and vertical planar manipulators have preferred to use this type of kinematic arrangements. Therefore, out of these seven kinematic configurations (RRR, PRP, RPP, PPR, PRR, RRP and RPR), only three of them, namely PRP, PRR, and PPR, are having a prismatic joint as its first joint, which reduces the total possible configurations to $3^3 = 27$. Additionally, most of the available designs of the PPMs are based on the symmetric topology (an equilateral triangle-shaped fixed base), which implies that all the three legs are equally spaced. Although the design with a symmetrical topology is better in several aspects, it is limited in usage due its complex kinematic relations and presence of singularities within the workspace.[1,2,3,9,21,23] On the other hand, the squared-shaped/U-shape fixed base (unsymmetrical topology) manipulators have some interesting features, namely larger workspace, higher positional accuracy, simple structure and ease of control. In the U-shape fixed base manipulators, there are two legs directed along the y or vertical axis and one leg is directed along the x or horizontal axis. From this condition, it seems that 9 configurations out of 27 are repeating; therefore, only 18 out of 27 configurations are the unique possible configurations in this manipulator family. Therefore, in order to identify the best manipulator from these 18 U-shape fixed base manipulators, a comparative performance study on these manipulators is performed in this paper.

As discussed in the above, the kinematic arrangements of all 27 possible manipulator configurations are given in Table I and the possible unique manipulator configurations (non-repeating kinematic arrangements) are given in Table II. Out of these unique possible configurations, a few of them are already analysed in the literature.[3,5–10,15,16,18,19,21–25] However, in order to identify the best manipulators out of these possible manipulators, a comparative kinematic performance study is performed and discussed in this section. In the kinematic performance analysis, the shape of the fixed platform of all these possible configurations is considered to be a U-shape fixed base. Each leg of the manipulator starts with an active prismatic joint that is connected to an equilateral triangle-shaped end-effector through the help of passive joints and links. In order to perform the detailed kinematic performance analyses, the kinematic relationships, namely the position and the velocity relationships of all the manipulators, are required. However, the manipulator kinematics is categorised into two parts, an inverse (or reverse) kinematics and a forward (or direct) kinematics. The inverse kinematic relationship involves the mapping from a known position of the output link of the manipulator to a set of input joint variables that will achieve that position. The forward kinematic relationship involves the mapping from a known set of input joint space variables to a pose (position and orientation) of the moving end-effector that results from those given inputs. Generally, as the number of closed kinematic loops in the manipulator increases, the difficulty of solving the forward kinematic relationships increases, while the difficulty of solving the inverse kinematic relationships decreases. In addition, the kinematic performance measures or quantifiers depend mainly on the Jacobian matrix. Therefore, the inverse kinematic (position) models of all the manipulators along with their Jacobian matrices are obtained and considered for the analysis. The kinematic performance of the manipulator can be quantified in a number of ways, and in this paper, it is quantified using the most prominent factor called

Table I. All possible configurations of the U-shape fixed base planar parallel manipulators starting with an active prismatic joint in each leg.

PPR-PPR-PPR	PPR-PPR-PRP	PPR-PRP-PPR
PRP-PPR-PPR	PPR-PPR-PRR	PPR-PRR-PPR
PRR-PPR-PPR	PPR-PRP-PRP	PRP-PPR-PRP
PRP-PRP-PPR	PPR-PRR-PRR	PRR-PRR-PPR
PRR-PPR-PRR	PPR-PRP-PRR	PPR-PRR-PRP
PRP-PPR-PRR	PRR-PRP-PPR	PRR-PPR-PRP
PRP-PRR-PPR	PRR-PRR-PRR	PRP-PRP-PRP
PRP-PRP-PRR	PRP-PRR-PRP	PRR-PRP-PRP
PRR-PRR-PRP	PRR-PRP-PRR	PRP-PRR-PRR

Table II. All non-repeating unique configurations of the U-shape fixed base planar parallel manipulators starting with an active prismatic joint in each leg.

PPR-PPR-PPR	PPR-PPR-PRP	PRP-PPR-PPR
PPR-PPR-PRR	PRR-PRR-PRP	PRP-PRR-PRR
PRR-PPR-PPR	PPR-PRP-PRP	PRP-PPR-PRP
PPR-PRP-PRR	PPR-PRR-PRR	PRR-PRR-PPR
PRP-PPR-PRR	PRR-PRP-PPR	PRR-PRR-PRR
PRP-PRP-PRR	PRR-PRP-PRP	PRP-PRP-PRP

kinematic isotropy. The isotropy corresponding to the inverse of the condition number is defined by the ratio of the minimum singular value to the maximum of the inverse Jacobian, and evaluates the workspace quality and prefers a sphere-like shape, i.e., unity.

2.1. Geometrical and kinematic arrangements of the U-shape fixed base planar parallel manipulators

The frame arrangements of the U-shape fixed base PPMs (as mentioned in Table II) are presented in Fig. 1(a)–(r). Each configuration of the manipulators has a mobile platform connected to a fixed platform through the help of three independent kinematic legs consist of three, 1-DOF joints starting with an active prismatic joint. The frame arrangement made with the help of a fixed reference O, and a moving reference Q attached to the end-effector. These frames are helpful to describe the kinematic (pose) model of the manipulator through the help of joint and link parameters. The shape of the end-effector is considered as an equilateral triangle whose side length is a and the height is h, and connected to the fixed platform via three kinematic legs, and their active joint displacements are denoted as $\boldsymbol{r}_i$ ($i = 1, 2, 3$). The link length of the connecting members from the active joint to the end-effector is denoted as l_j ($j = 1, 2, 3$). s is the width or span and h^* is the height of the fixed platform. The orientation angle (the z-axis rotation) of the mobile platform is presented by θ, and the design angles of certain configurations, namely PRR legs, are denoted by θ_k ($k = 1, 2, 3, 4$).

The kinematic configurations shown in Fig. 1(a)–(r) are composed of only three kinematic legs namely PPR, PRP, PRR due to the condition that the first joint of each leg should be a prismatic joint. In the case of PRR kinematic leg, an active prismatic joint is connected to the mobile platform (work table) by using two revolute joints. The configurations that are having two passive rotary joints in any of the legs (i.e., PRR leg) are shown in Fig. 1(c), (e), (f) and (i)–(r); in these cases, the link lengths of the first link are denoted as l_m ($m = 1, 3, 5$) and the second link are denoted as l_n ($n = 2, 4, 6$). In the PRR leg, the first link is attached rigidly to an active prismatic joint with a certain angle (design angle) to enhance better workspace and the kinematic design performance of the manipulator. The first end of the second link is attached with the first link by a revolute joint and the other end is attached with the mobile platform through a revolute joint. So, the first design angle between the horizontal axis and the first link is represented as θ_{k_1} ($k_1 = 1,\ 3$) and shown in Fig. 1(c), (e), (f) and (i)–(r), and the second design angle between these first and second link is represented as θ_{k_2} ($k_2 = 2,\ 4$) and shown in Fig. 1(c), (e), (f) and (i)–(r). The PPR kinematic leg consists of an active prismatic joint, followed

https://doi.org/10.1017/S0263574718000267 Published online by Cambridge University Press

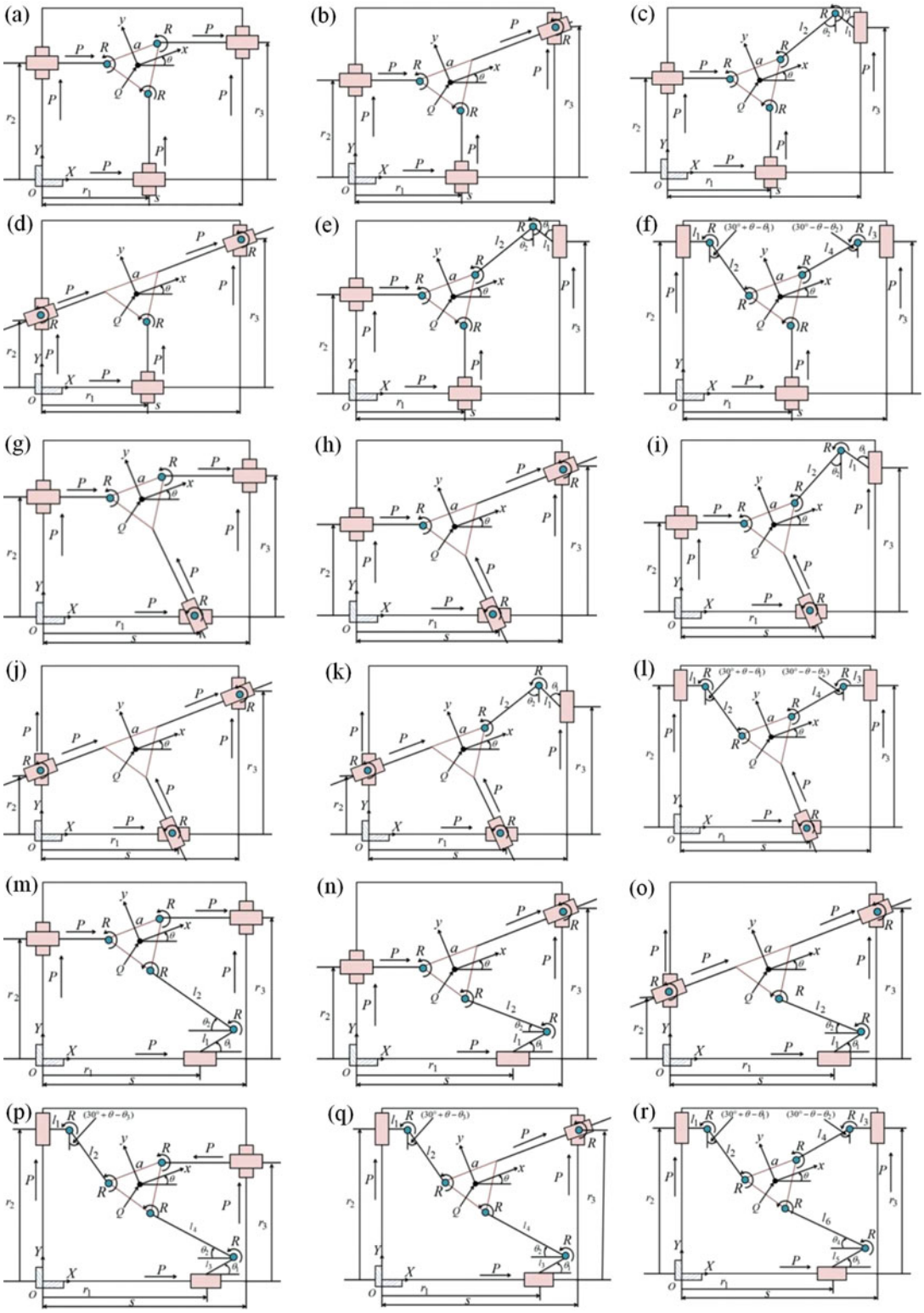

Fig. 1. Frame diagrams of all the possible U-shape fixed base planar parallel manipulators. (a) PPR-PPR-PPR. (b) PPR-PPR-PRP. (c) PPR-PPR-PRR. (d) PPR-PRP-PRP. (e) PPR-PRP-PRR. (f) PPR-PRR-PRR. (g) PRP-PPR-PPR. (h) PRP-PPR-PRP. (i) PRP-PPR-PRR. (j) PRP-PRP-PRP. (k) PRP-PRP-PRR. (l) PRP-PRR-PRR. (m) PRR-PPR-PPR. (n) PRR-PPR-PRP. (o) PRR-PRP-PRP. (p) PRR-PRR-PPR. (q) PRR-PRR-PRP. (r) PRR-PRR-PRR.

https://doi.org/10.1017/S0263574718000267 Published online by Cambridge University Press

by a passive prismatic joint and a revolute joint. The PRP kinematic leg consists of an active prismatic joint followed by a revolute joint and a passive prismatic joint.

These 18 manipulators have 3-DOF, and all three controllable inputs are considered as translation (prismatic) inputs for the design and performance analysis.

2.2. Kinematic performance measure

In this section, a brief introduction about the kinematic performance measure, specifically, the kinematic isotropy, is discussed and presented. During the kinematic performance study, it was found that one of the manipulators, namely PPR-PRP-PRP manipulator, has singularity when $\theta \geq 45^\circ$. Therefore, for better understanding and appropriate comparisons, the end-effector orientation angle range has been restricted as $\theta \leq 45^\circ$ for the entire kinematic analysis, i.e., θ is varied between 0° and 45°. Moreover, in most of the manipulator configurations, the task-space position y is dependent and does not influence the kinematic performance measure. The isotropy is the local performance index that evaluates the accuracy, velocity and rigidity of the manipulator between the joint space and the task-space variables. Superior isotropy of the manipulator exists in the case of singularity-free configuration. The kinematic isotropy value ranges from 0 to 1. The normalised kinematic isotropy of the manipulator is the best when it is equal to 1. For the accurate system performance, the kinematic isotropy values should be higher for the manipulators. Figures 3–5 show the comparative plot variation of the above-mentioned performance index with respect to the orientation angle θ of the manipulators. Formulations for as the kinematic isotropy for the non-redundant manipulator[5,8,19,20,23,30,37–41] are given as follows:

$$\omega_I = \frac{1}{\|\mathbf{J}_h\| \left\|\mathbf{J}_h^{-1}\right\|} \tag{1}$$

where $\|\mathbf{J}_h\| = \sqrt{tr\left(\frac{\mathbf{J}_h \mathbf{J}_h^T}{3}\right)}$, ω_I is the kinematic isotropy of the manipulator and $tr(\bullet)$ is the trace of the matrix. $\mathbf{J_h}$ is the homogeneous (normalised) Jacobian matrix of the manipulator. However, because the task space vector includes components that are of a different nature, namely two linear velocities and one angular velocity, the entries of matrix $\mathbf{J}$ will bear different physical units for all the 3-DOF PPMs discussed in the present paper. Thus, this dimensional inhomogeneity can be resolved by introducing a normalising characteristic length.[3,6,8,31] To render the matrix $\mathbf{J}$ homogeneous, each term of the third column of matrix $\mathbf{J}$ is divided by the characteristic length R_a[3,6,8,31] as shown in Fig. 2. Explanation for the mentioned approach is presented here for PPR-PPR-PPR PPM and the same approach has been applied for all other manipulators discussed in the present paper.

The end-effector of the manipulator is an equilateral triangle shape as discussed above, which contains a circle, with a radius r_a as shown in Fig. 2. The centres of the rotational joints are on the vertices of the triangle. The active prismatic joints can travel on the sides of the outer square shape fixed base that contains a circle of radius R_a. The end-effector of the manipulator has the pose of translation (x, y) and rotation θ from the reference point O. The inverse kinematic relations and Jacobian matrices of PPR-PPR-PPR manipulator are derived and discussed here. As shown in Fig. 2, manipulator have three translational inputs (r_1, r_2 and r_3) and are considered as joint space variables (joint displacements). The end-effector position and orientation (pose), namely x, y and θ, are considered as the task space variables. From Fig. 2, it is clearly noted that all the active prismatic joints are mounted on three sides of square shape (fixed) base; in other words, the active prismatic joints are arranged in U shape.

The task space variables, i.e., translation motions (horizontal and vertical) and orientation of the end-effector, are dependent on the horizontal prismatic joint (r_1) and the vertical prismatic joints (r_2 and r_3) due to the coupled kinematic arrangement of the manipulator. Inverse kinematic relation addresses the vector of joint space displacements $\mathbf{q} = [\, r_1 \; r_2 \; r_3 \,]^T$ in terms of Cartesian space vector of displacements (pose) $\boldsymbol{\mu} = [\, x \; y \; \theta \,]^T$, i.e., $\mathbf{q} = fun(\boldsymbol{\mu})$, where, $fun(\boldsymbol{\mu})$ is the function of Cartesian space displacements (variables). Additionally, differentiating the inverse kinematic solution with respect to time gives the velocity relation of the manipulator, and the relation of joint space velocities to the task space velocities is given as follows:

$$\dot{\mathbf{q}} = \mathbf{J}(\boldsymbol{\mu})\, \dot{\boldsymbol{\mu}} \tag{2}$$

https://doi.org/10.1017/S0263574718000267 Published online by Cambridge University Press

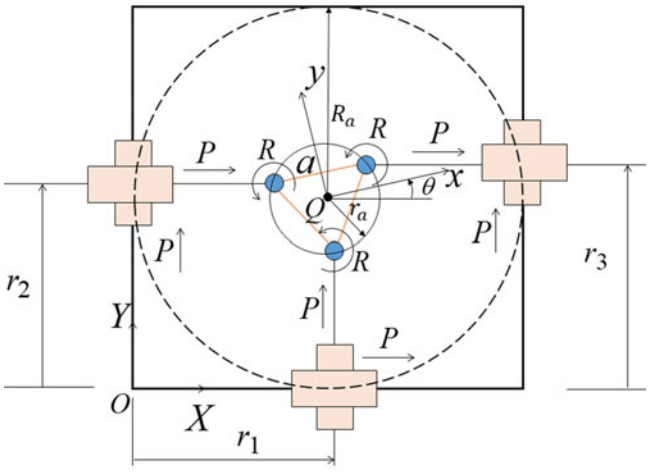

Fig. 2. Coordinate system for PPR-PRP-PRP PPM.

where $\dot{\boldsymbol{\mu}} = [\dot{x}\ \dot{y}\ \dot{\theta}\ ]^T$ is the vector of Cartesian (task space) velocities of the manipulator, and $\dot{\mathbf{q}} = [\dot{r}_1\ \dot{r}_2\ \dot{r}_3\ ]^T$ is the vector of active prismatic joint (joint space) velocities of the manipulator. $\mathbf{J}(\boldsymbol{\mu})$ is the Jacobian (velocity transformation/mapping) matrix of the manipulator, which maps Cartesian space velocities to joint space velocities. The inverse kinematic relations and the Jacobian matrix of PPR-PPR-PPR manipulator are given as follows:

$$\mathbf{q} = \begin{bmatrix} x + \frac{2h}{3}\sin\theta \\ y + \frac{h}{3}\cos\theta - \frac{a}{2}\sin\theta \\ y + \frac{h}{3}\cos\theta + \frac{a}{2}\sin\theta \end{bmatrix} = fun\,(\boldsymbol{\mu}) \tag{3}$$

$$\mathbf{J}\,(\boldsymbol{\mu}) = \begin{bmatrix} 1 & 0 & \frac{2h}{3}\cos\theta \\ 0 & 1 & -\frac{h}{3}\sin\theta - \frac{a}{2}\cos\theta \\ 0 & 1 & -\frac{h}{3}\sin\theta + \frac{a}{2}\cos\theta \end{bmatrix} \tag{4}$$

The elements of the Jacobian of Eq. (4) do not have the same dimension as discussed above. First two columns corresponding to translation are dimensionless, whereas the last column corresponding to rotation has the dimension of length. By making the third column dimensionless, a homogeneous Jacobian with non-dimensional elements is obtained the use of above discussed approach (characteristics length[3,6,8,31]):

$$\mathbf{J_h} = \mathbf{J}\,(\boldsymbol{\mu}) \begin{bmatrix} 1 & 0 & 0 \\ 0 & 1 & 0 \\ 0 & 0 & \frac{1}{R_a} \end{bmatrix} \tag{5}$$

2.3. Geometric parameters of manipulators

In this section, the kinematic isotropy of all the manipulator configurations are obtained, analysed and compared with the help of the above-mentioned approach. This analysis helps to obtain the valuable information about the kinematic behaviour of these manipulators, such as positioning accuracy, rigidity mapping characteristics and quality of the workspace. For the comparative study, a certain geometrical parameter is considered and is listed in Tables III and IV. To demonstrate the kinematic performance of the manipulators, the numerical simulations have been performed by running the computer-based codes through the help of the obtained kinematic models and Jacobian matrices. For obtaining a common workspace and better comparison, a certain set of design angles, link lengths, fixed

https://doi.org/10.1017/S0263574718000267 Published online by Cambridge University Press

Table III. Common geometrical parameters for all the 18 U-shape fixed base manipulators.

Dimensions of the end-effector (equilateral triangle-shaped)		
Parameters	Description	Values
a	Side length	160 (mm)
h	Height	138.5 (mm)
Dimensions of the fixed platform (U-shape)		
Parameters	Description	Values
s	Width	1000 (mm)
h^*	Height	1000 (mm)
Active prismatic actuators stroke length		
Parameters	Description	Values
r_1	Actuator stroke length along the x-axis	1000 (mm)
r_2	Actuator stroke length along the y-axis	1000 (mm)
r_3	Actuator stroke length along the z-axis	1000 (mm)
Parameters for the analyses of performance indices		
x	Desired task-space variable along the x-axis	0−1000 (mm)
y	Desired task-space variable along the y-axis	500 (mm)
θ	Desired task-space variable, orientation angle θ about the z-axis	0−45°

Table IV. Structural and geometrical parameters of the different manipulator configurations.

Link length and design angles					
Configurations	l_1 (mm)	l_2(mm)	l_3 (mm)	l_4 (mm)	θ_1
PPR-PPR-PRR	400	700	NA	NA	45°
PPR-PRP-PRR	400	700	NA	NA	45°
PPR-PRR-PRR	80	1000	80	1000	NA
PRP-PPR-PRR	400	700	NA	NA	45°
PRP-PRP-PRR	400	700	NA	NA	45°
PRP-PRR-PRR	80	1000	80	1000	NA
PRP-PRP-PRR	400	700	NA	NA	45°
PRR-PPR-PPR	400	700	NA	NA	45°
PRR-PPR-PRP	400	700	NA	NA	45°
PRR-PRP-PRP	400	700	NA	NA	45°
PRR-PRR-PPR	400	700	NA	NA	45°
PRR-PRR-PRP	80	1000	80	1000	NA
PRR-PRR-PRR	80	1000	80	1000	NA

platform and mobile platform sizes is considered for the performance analyses, and these configuration parameters are listed in Tables III and IV.

For the better comparison and to obtain the consistent results, the total analysis is performed by varying only the variables x and θ. For the kinematic performance analysis, the task-space variable x is varied between 0 mm and 1000 mm, the task-space variable y is considered as a constant and the value of y is considered as 500 mm. The kinematic performance analysis results in terms of the kinematic isotropy contour plots are presented in Figs. 3–5.

2.4. Comparative kinematic performance analyses of the U-shape fixed base planar parallel manipulators

The numerical values of the kinematic isotropy of the 18 U-shape fixed base manipulator configurations are presented in Table V. It consists of maximum, minimum and mean of the isotropy values. Figures 3–5 show the isotropy for all manipulator configurations in terms of contour plots. From Figs. 3–5 and Table V, it is observed that that the maximum values of the isotropy of the PPR-PRP-PRP, PRP-PRP-PRP, PRP-PRP-PRR and PRR-PRP-PRP manipulator configurations are higher compared to the others and calculated as 0.94, 0.82, 0.84 and 0.94, respectively; however, the mean values of

https://doi.org/10.1017/S0263574718000267 Published online by Cambridge University Press

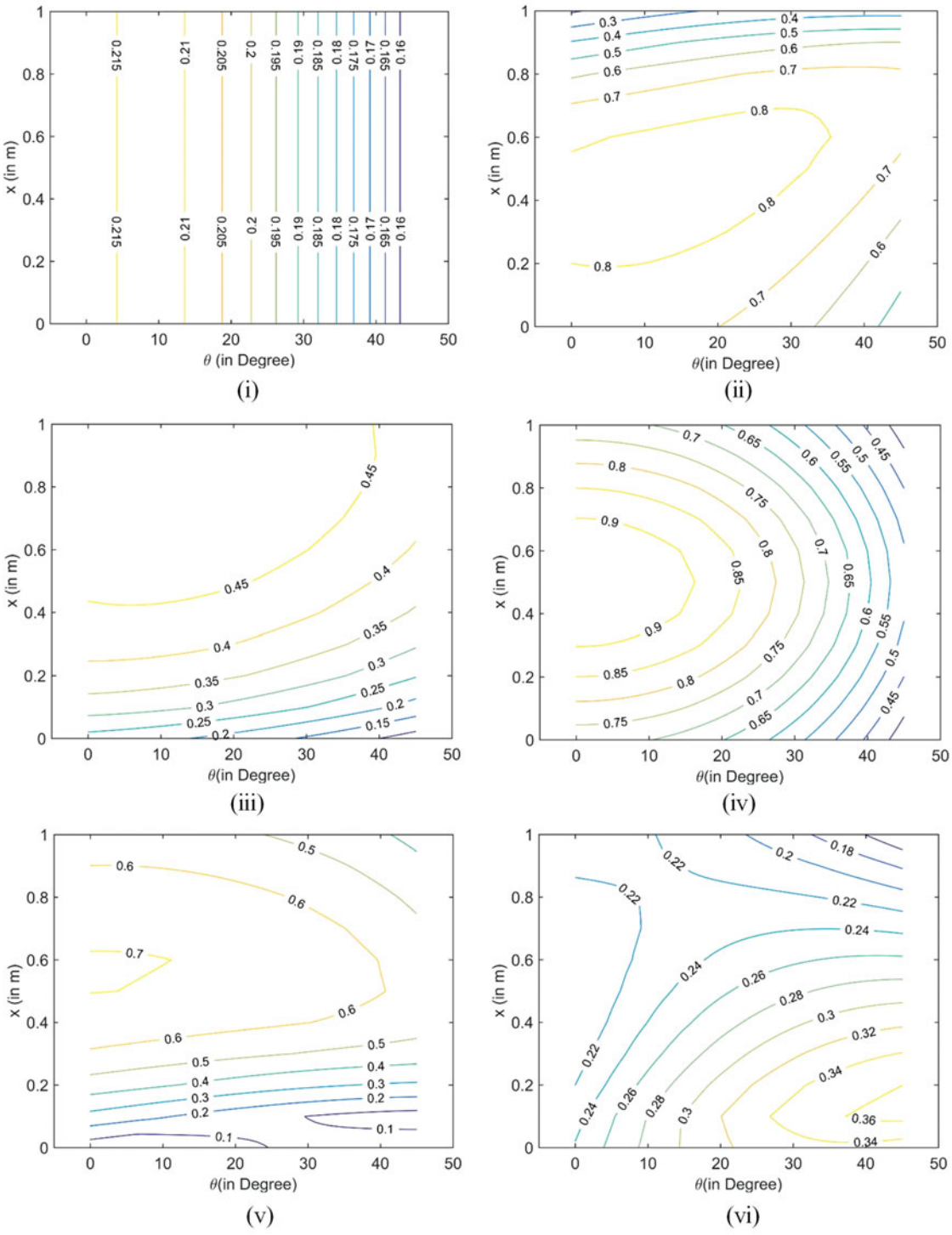

Fig. 3. The kinematic isotropy contour plots of the U-shape fixed base manipulators. (i) PPR-PPR-PPR. (ii) PPR-PPR-PRP. (iii) PPR-PPR-PRR. (iv) PPR-PRP-PRP. (v) PPR-PRP-PRR. (vi) PPR-PRR-PRR.

the isotropy of the PPR-PRP-PRP, PRP-PRP-PRP and PRR-PRP-PRP manipulator configurations are higher than the other manipulators, and their values are 0.71, 0.71 and 0.75, respectively. Therefore, only the top-three manipulator configurations, namely PPR-PRP-PRP, PRP-PRP-PRP and PRR-PRP-PRP, are considered for the further analyses.

https://doi.org/10.1017/S0263574718000267 Published online by Cambridge University Press

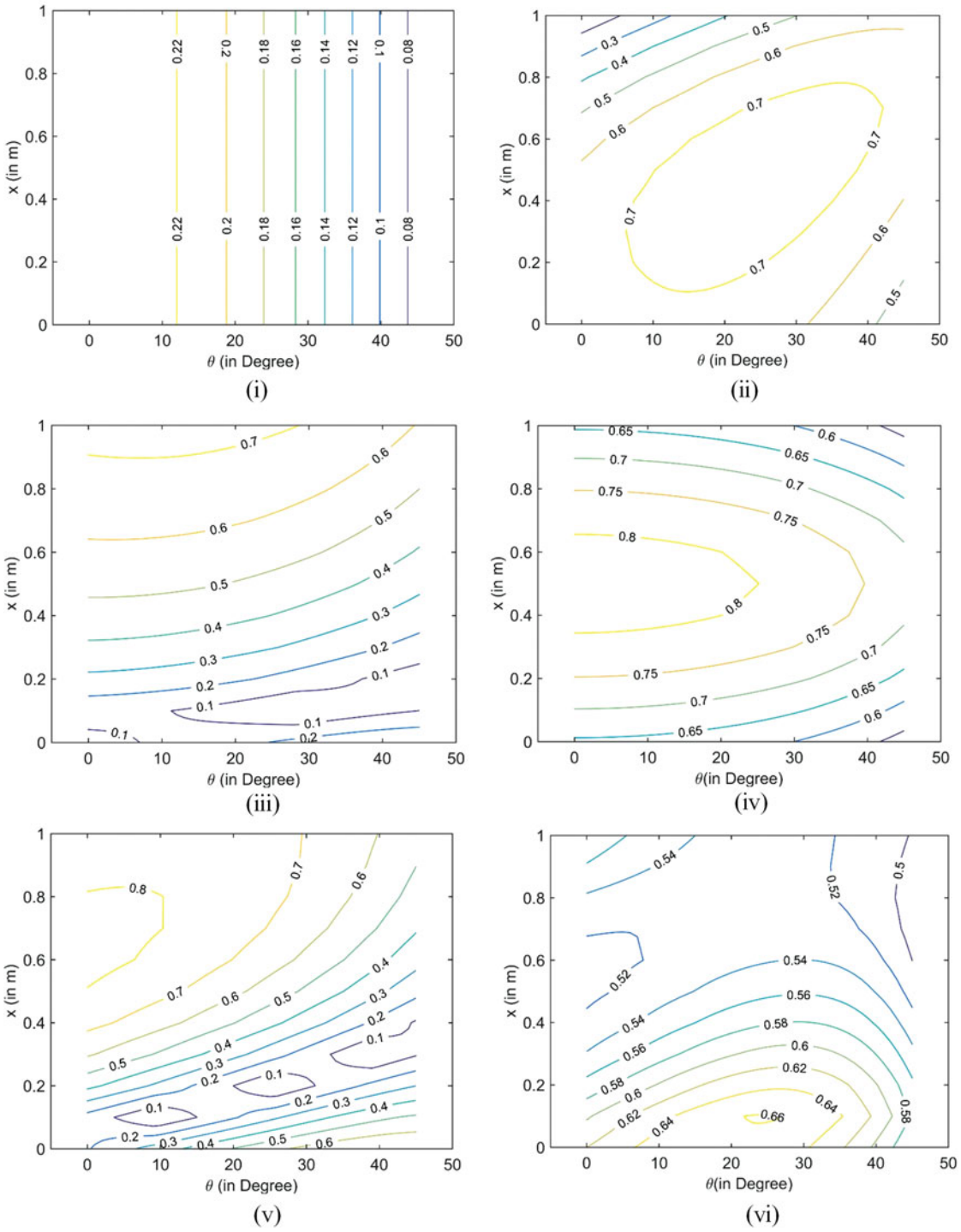

Fig. 4. The kinematic isotropy contour plots of the U-shape fixed base manipulators. (i) PRP-PPR-PPR. (ii) PRP-PPR-PRP. (iii) PRP-PPR-PRR. (iv) PRP-PRP-PRP. (v) PRP-PRP-PRR. (vi) PRP-PRR-PRR.

2.5. Kinematic analysis of the top-three U-shape fixed base manipulator configurations

As discussed in the earlier sections, a few of the manipulator configurations, namely PPR-PRP-PRP (PreXYT) and PRP-PRP-PRP (3PRP Hephaist) configurations, are already discussed in the literature[3,15,17] and are commercially available with different structural designs (for example, all three legs of the manipulators are connected to a single point of the end-effector, which is presented in the paper as square-/rectangular-shaped end-effector). The PPR-PRP-PRP (2PRP-PPR) manipulator's

https://doi.org/10.1017/S0263574718000267 Published online by Cambridge University Press

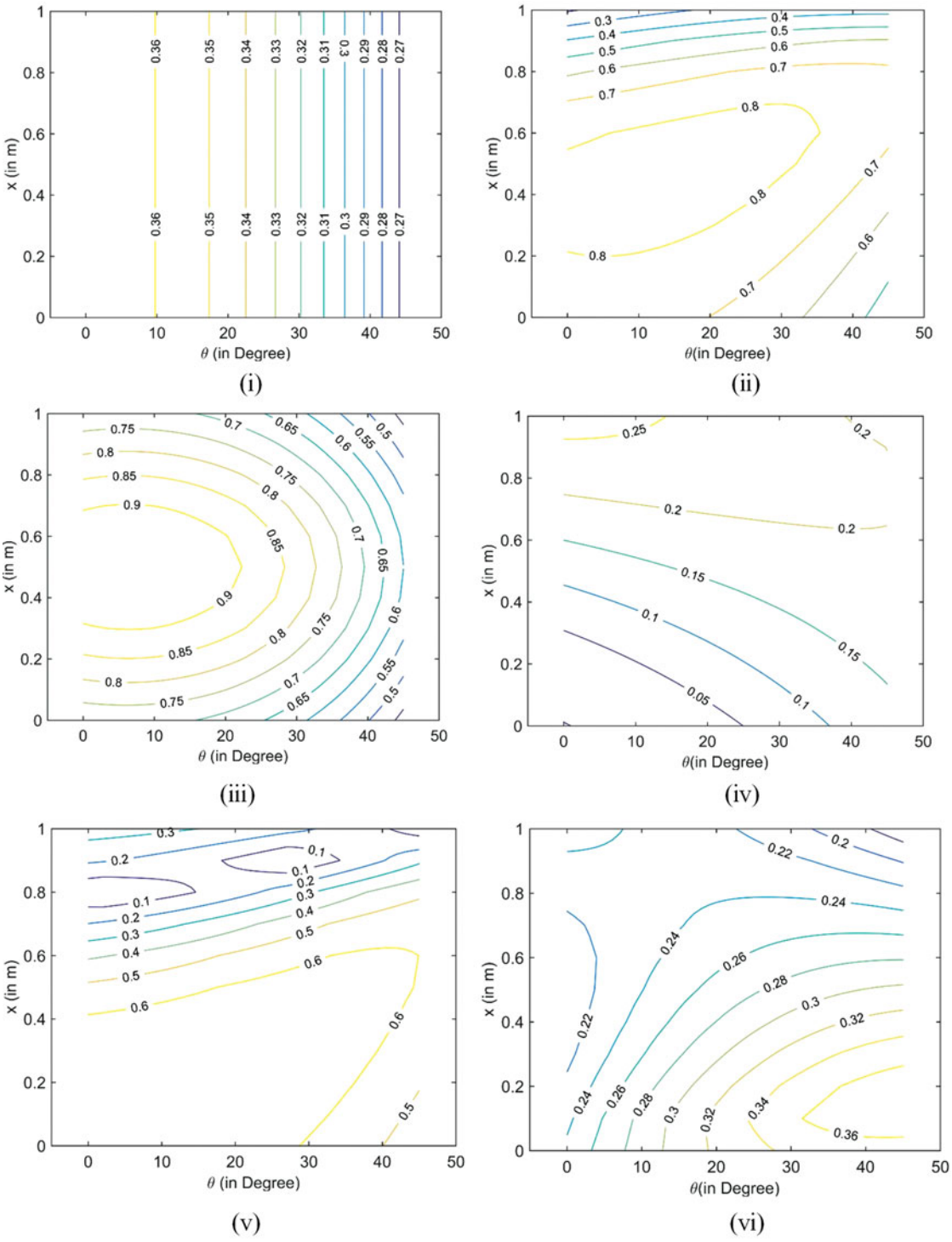

Fig. 5. The kinematic isotropy contour plots of the U-shape fixed base manipulators. (i) PRR-PPR-PPR. (ii) PRR-PPR-PRP. (iii) PRR-PPR-PRR. (iv) PRR-PRP-PRP. (v) PRR-PRP-PRR. (vi) PRR-PRR-PRR.

structural arrangement had a few technical issues, namely misalignment and cantilever effects on its PPR leg (which are affecting the overall system performance). To overcome these issues, an additional PPR leg (as a slider or roller support) has been added to the PPR-PRP-PRP configuration to enhance its structural stability, rigidity and stiffness, and to reduce the misalignment and cantilever effects of the manipulator (the modified design as a solid model is presented in Fig. 6). The PPR leg (with a roller or slider support) is added in such a way that it does not increase the DOF of the manipulator. It

https://doi.org/10.1017/S0263574718000267 Published online by Cambridge University Press

Table V. Numerical values of the kinematic isotropy of the 18 U-shape fixed base manipulator configurations.

	Kinematic isotropy		
Configurations	Max.	Min.	Mean
PPR-PPR-PPR	0.21	0.15	0.19
PPR-PPR-PRP	0.80	0.18	0.68
PPR-PPR-PRR	0.49	0.07	0.39
PPR-PRP-PRP	0.94	0.35	0.71
PPR-PRP-PRR	0.70	0.00	0.48
PPR-PRR-PRR	0.36	0.14	0.25
PRP-PPR-PPR	0.23	0.07	0.17
PRP-PPR-PRP	0.75	0.11	0.62
PRP-PPR-PRR	0.72	0.00	0.42
PRP-PRP-PRP	0.82	0.51	0.71
PRP-PRP-PRR	0.82	0.00	0.51
PRP-PRR-PRR	0.66	0.48	0.56
PRR-PPR-PPR	0.36	0.26	0.33
PRR-PPR-PRP	0.84	0.18	0.68
PRR-PRP-PRP	0.94	0.43	0.75
PRR-PRR-PPR	0.26	0.00	0.15
PRR-PRR-PRP	0.69	0.00	0.48
PRR-PRR-PRR	0.38	0.16	0.27

is observed from the analyses and the prior art that PPR-PRP-PRP and PRP-PRP-PRP configurations presented in this paper are in association with an equilateral triangle-shaped (means all three legs of the manipulators are connected to the end-effector through the help of three points) and a squared-shaped (as mentioned above) mobile platform configuration, and their design and the kinematic relationships are different from the previous works. It is also observed that previous analyses on the top-three manipulators are performed using an equilateral triangle-shaped end-effector, and their kinematic relationships were fully coupled, as shown in Tables VI–VIII.

However, from the literature, it is found that for a squared-shaped end-effector (all three legs of the manipulator are connected with the end-effector platform on a point), the kinematic relations may be partially decoupled.[3,15,17] Therefore, in order to investigate further, one more kinematic performance analysis is performed for these top-three manipulators. But, in this analysis, the end-effector of the manipulator is connected to the legs on a point, which is presented as a squared-shaped end-effector instead of an equilateral triangle-shaped end-effector (legs on the fixed base connected to the end-effector with three distinct point forming equilateral triangle), as shown in Figs. 6–8. The kinematic and structural arrangements of these top-three PPR-PRP-PRP, PRP-PRP-PRP and PRR-PRP-PRP manipulators with the squared-shaped end-effector are depicted in Figs. 6–8, respectively, where all three legs are connected on a single point. Here onwards, the manipulator configurations PPR-PRP-PRP, PRP-PRP-PRP and PRR-PRP-PRP will be addressed as configuration-1, configuration-2 and configuration-3, respectively.

Two of the legs of the configuration-1 are having the prismatic-revolute-prismatic configuration and other one leg has prismatic-prismatic-revolute configuration. All the three legs of the configuration-2 have the prismatic-prismatic-revolute configuration. Two of the legs of the configuration-3 having the prismatic-revolute-prismatic configuration and other one leg has prismatic-revolute-revolute configuration. Design angle θ_1 (in the case of configuration-3) between link l_1 and the active prismatic joint r_1 is a fixed angle and affects the kinematic performance of the manipulator. In the present paper, the design angle θ_1 is assumed to be 45°, since it gives the favourable performance measures and good singularity-free workspace.[42] Inverse kinematics relations and Jacobian matrices of the configuration-1, configuration-2 and configuration-3 for both end-effector shapes (equilateral triangle and square) are derived and presented in Tables VI–VIII.

2.5.1. Comparative kinematic isotropy of the U-shape fixed base planar parallel manipulators for two different end-effector connections. In order to compare the kinematic isotropy of the above-mentioned

https://doi.org/10.1017/S0263574718000267 Published online by Cambridge University Press

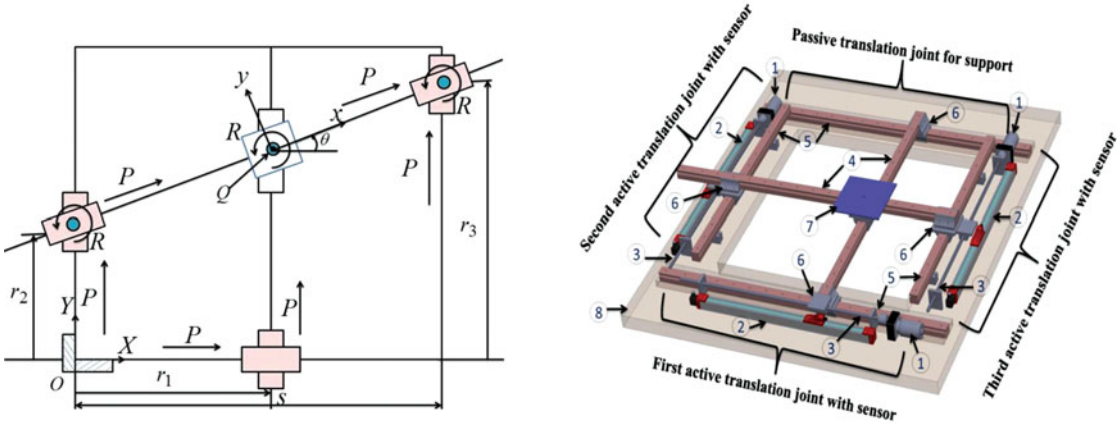

Fig. 6. Frame diagram and performance indices of the PPR-PRP-PRP manipulator (configuration-1). (a) 1: DC motor; (b) 2: Linear potentiometer (Sensor); (c) 3: Coupler and ball screw arrangement for linear motion; (d) 4: Passive link; (e) 5: Linear guide rail; (f) 6: Slider block or translation joint; (g) 7: End-effector (Mobile platform); (h) 8: Base.

three manipulators (as shown in Figs. 6–8), the geometrical and physical parameters are considered as discussed earlier in this paper. For the earlier analyses, the end-effector shape is considered as an equilateral triangle. However, in the present comparative analyses, it is considered as a square shape with a side of 100 mm (this does not affect the analyses at any instant, since all the three limbs are connected to the end-effector at a single point). Therefore, the comparative results of these top-three configurations with two different end-effector connections to the legs are presented in Figs. 3(iv), 4(iv) and 5(iii) (equilateral triangle end-effector), Fig. 9 (square end-effector) and Table X.

2.5.2. Workspace of the top-three manipulators. Workspaces for these top-three PPMs are analysed and presented for the end-effector orientation $[-15^\circ, +15^\circ]$ as shown in Fig. 10. The numerical values of the ratio of the workspace to the total space required for configuration-1, configuration-2 and configuration-3 are presented as 0.40, 0.13 and 0.35, respectively. Here, the total space required is defined as the required space accommodating the mechanism without hindrance; basically, it is the outer boundary made by the system components.

It is found from the analysis that configuration-1 is clearly outperforming in providing higher workspace to total area required (red colour region as shown in Fig. 10(a), (c) and (e)) ratio compared to the other configurations due to its partially decoupled kinematic relations and simple structure.

From Figs. 3–5 and Tables V and X, a few points are observed and are listed as follows:

- The isotropy values of the configurations, namely configuration-1 and configuration-3 are decreased with the increase of orientation angle θ. Similarly, in the configuration-2 the isotropy indices are higher when the manipulator's end effector lies at the centre of its workspace (i.e., for $x = 500$, $y = 500$ and orientation angle $\theta = 0^\circ$ to 45°).
- The kinematic isotropy is decreasing for configuration-1 and configuration-3 with the increase of orientation angle θ. The isotropy of configuration-2 is more dependent on the task-space variables x and y due to its structural arrangement. Therefore, the dexterity of configuration-2 is higher at the mid position of its workspace (i.e., 500 mm, 500 mm).
- The isotropy values of configuration-3 (in association with square shape base end-effector) are higher among others. This implies that the load-bearing capacity and the dexterity of the configuration-3 manipulator are higher compared to others.
- PRR legs of the manipulators are having flexibility in terms of their design angle (fixed angle) and the link length attached with the active prismatic joint and affect the performance of the manipulator.
- In the present analysis, in order to make consistent comparison, the values of the link length and the design angle of the PRR leg are considered as given in Table IV. These values are considered based on the near optimal analysis performed through the help of workspace and isotropy analyses, and the design optimisation is performed through the help of genetic algorithms. But, it was not the main objective or interest of the current manuscript. So, further design optimisation aspects of this

https://doi.org/10.1017/S0263574718000267 Published online by Cambridge University Press

Table VI. Kinematic solutions of the Configuration-1 with two different end-effector connections to the legs.

Configuration	End-effector connection to the legs (two different shape)	Inverse kinematic equations	Jacobian matrix
Configuration-1 (PPR-PRP-PRP)	Equilateral triangle (Fig. 1(d))[1,3,4,15]	$\mathbf{q} = \begin{bmatrix} x + \frac{2h}{3}\sin\theta \\ y + \frac{2h}{3}\sin(30^\circ - \theta) - s_1 \\ y + \frac{2h}{3}\sin(30^\circ + \theta) + s_2 \end{bmatrix} = fun(\boldsymbol{\mu})$ where, $s_1 = \left(x - \frac{2h}{3}\cos(30^\circ - \theta)\right)\tan\theta$ $s_2 = \left(s - x - \frac{2h}{3}\cos(30^\circ + \theta)\right)\tan\theta$	$\mathbf{J}(\boldsymbol{\mu}) = \begin{bmatrix} 1 & 0 & \frac{2h}{3}\cos\theta \\ -\tan\theta & 1 & s_3 \\ -\tan\theta & 1 & s_4 \end{bmatrix}$ where, $E_1 = \left(\frac{2h}{3}\sin(30^\circ + \theta)\right)\tan\theta$ $F_1 = \sec^2\theta\left(s - x - \frac{2h}{3}\cos(30^\circ + \theta)\right)$ $E_2 = \left(\frac{2h}{3}\sin(30^\circ - \theta)\right)\tan\theta$ $F_2 = \sec^2\theta\left(x - \frac{2h}{3}\cos(30^\circ - \theta)\right)$ $s_3 = -\frac{2h}{3}\cos(30^\circ - \theta) + E_2 - F_2$ $s_4 = \frac{2h}{3}\cos(\theta + 30^\circ) + E_1 + F_1$
	Square (Fig. 4)[1,3,4,15]	$\mathbf{q} = \begin{bmatrix} x \\ y - x\tan\theta \\ y + (s - x)\tan\theta \end{bmatrix} = fun(\boldsymbol{\mu})$	$\mathbf{J}(\boldsymbol{\mu}) = \begin{bmatrix} 1 & 0 & 0 \\ -\tan\theta & 1 & -x\sec^2\theta \\ -\tan\theta & 1 & (s - x)\sec^2\theta \end{bmatrix}$

Table VII. Kinematic solutions of the Configuration-2 with two different end-effector connections to the legs.

Configuration	End-effector connection to the legs (two different shapes)	Inverse kinematic equations	Jacobian matrix
Configuration-2 (PRP-PRP-PRP)	Equilateral triangle (Fig. 1(j))[1,3,4,15]	$\mathbf{q} = \begin{bmatrix} x + y\tan\theta \\ y + \frac{2h}{3}\sin(30^\circ - \theta) - s_1 \\ y + \frac{2h}{3}\sin(30^\circ + \theta) + s_2 \end{bmatrix} = fun(\boldsymbol{\mu})$	$\mathbf{J}(\boldsymbol{\mu}) = \begin{bmatrix} 1 & \tan\theta & y\sec^2\theta \\ -\tan\theta & 1 & s_3 \\ -\tan\theta & 1 & s_4 \end{bmatrix}$
	Square (Fig. 5)[1,3,4,15]	$\mathbf{q} = \begin{bmatrix} x + y\tan\theta \\ y - x\tan\theta \\ y + (s - x)\tan\theta \end{bmatrix} = fun(\boldsymbol{\mu})$	$\mathbf{J}(\boldsymbol{\mu}) = \begin{bmatrix} 1 & \tan\theta & y\sec^2\theta \\ -\tan\theta & 1 & -x\sec^2\theta \\ -\tan\theta & 1 & (s - x)\sec^2\theta \end{bmatrix}$

Note: $\dot{\boldsymbol{\mu}} = [\,\dot{x}\ \dot{y}\ \dot{\theta}\,]^{\mathrm{T}}$ is the vector of Cartesian (task space) velocities of the manipulator. $\dot{\mathbf{q}} = [\,\dot{r}_1\ \dot{r}_2\ \dot{r}_3\,]^{\mathrm{T}}$ is the vector of active prismatic JOINT (joint space) velocities of the manipulator. $\mathbf{J}(\boldsymbol{\mu})$ is the Jacobian (velocity transformation/mapping) matrix of the manipulator that maps Cartesian space velocities to joint space velocities.

Table VIII. Kinematic solutions of the Configuration-3 with two different end-effector connections to the legs.

Configuration	End-effector connection to the legs (two different shapes)	Inverse kinematic equations	Jacobian matrix
Configuration-3 (PRR-PRP-PRP)	Equilateral triangle (Fig. 1(o))	$\mathbf{q} = \begin{bmatrix} x + \frac{2h}{3}\cos(90^\circ - \theta) + s_3 \\ y + \frac{2h}{3}\sin(30^\circ - \theta) - s_1 \\ y + \frac{2h}{3}\sin(30^\circ + \theta) + s_2 \end{bmatrix} = fun(\boldsymbol{\mu})$ where, $\theta_2 = \sin^{-1}\left(\frac{y - \frac{2h}{3}\sin(90^\circ - \theta) - l_1\sin\theta}{l_2}\right)$ $s_5 = l_2\cos\theta_2 - l_1\cos\theta_1$	$\mathrm{J}(\boldsymbol{\mu}) = \begin{bmatrix} 1 & \frac{s_6}{l_2} & \frac{2h}{3}\cos\theta + s_6 s_7 \\ -\tan\theta & 1 & s_3 \\ -\tan\theta & 1 & s_4 \end{bmatrix}$ where, $B_1 = y - \frac{2h}{3}\sin(90^\circ - \theta) - l_1\sin\theta_1$ $s_6 = -\left(\frac{-l_2\sin\theta_2}{\sqrt{1-(\frac{B_1}{l_2})^2}}\right)$ $s_7 = -\frac{\frac{2h}{3}\cos(90^\circ - \theta)}{l_2}$
	Square (Fig. 6)	$\mathbf{q} = \begin{bmatrix} x + l_2\cos\theta_2 - l_1\cos\theta_1 \\ y - x\tan\theta \\ y + (s - x)\tan\theta \end{bmatrix} = fun(\boldsymbol{\mu})$ where, $\theta_2 = a\tan 2(y - l_1\sin\theta_1,\ x - r_1 - l_1\cos\theta_1)$	$\mathbf{J}(\boldsymbol{\mu}) = \begin{bmatrix} 1 & \tan\theta_2 & 0 \\ -\tan\theta & 1 & -x\sec^2\theta \\ -\tan\theta & 1 & (s - x)\sec^2\theta \end{bmatrix}$

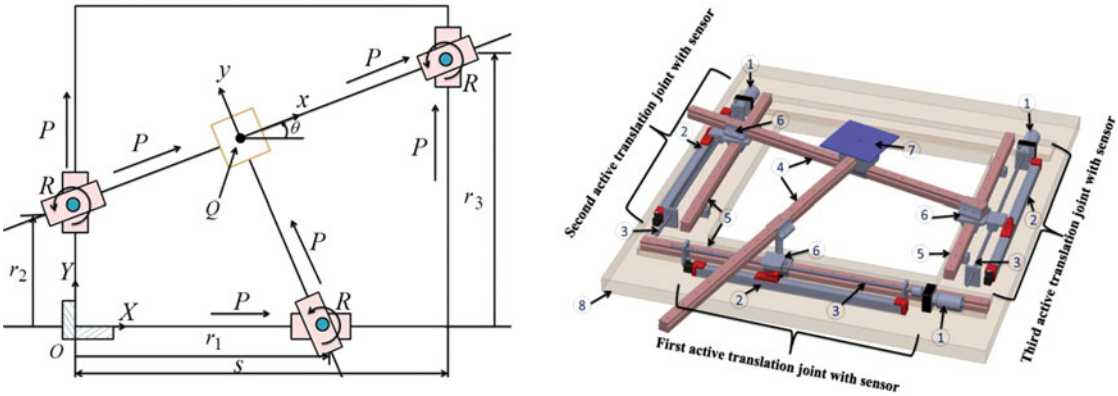

Fig. 7. Frame diagram and performance indices of the PRP-PRP-PRP manipulator (configuration-2). (a) 1: DC motor; (b) 2: Linear potentiometer (Sensor); (c) 3: Coupler and ball screw arrangement for linear motion; (d) 4: Passive link; (e) 5: Linear guide rail; (f) 6: Slider block or translation joint; (g) 7: End-effector (Mobile platform); (h) 8: Base.

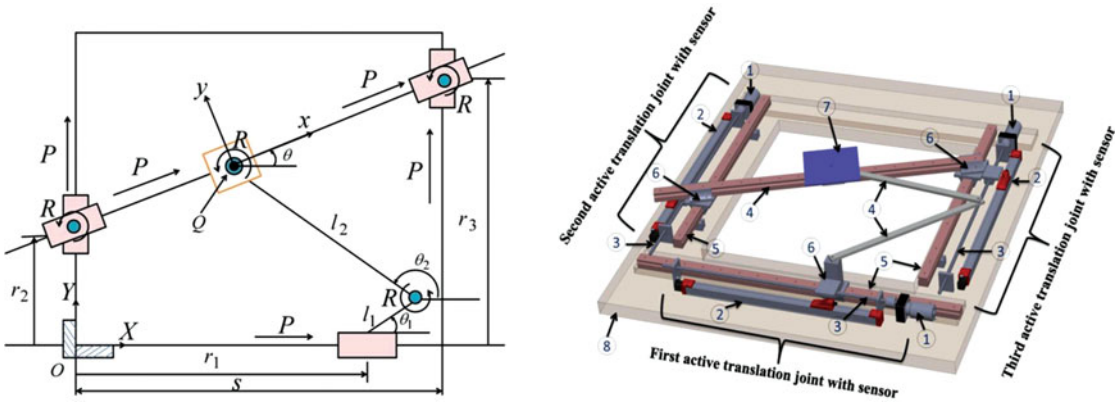

Fig. 8. Frame diagram and performance indices of the PRR-PRP-PRP manipulator (configuration-3). (a) 1: DC motor; (b) 2: Linear potentiometer (Sensor); (c) 3: Coupler and ball screw arrangement for linear motion; (d) 4: Passive link; (e) 5: Linear guide rail; (f) 6: Slider block or translation joint; (g) 7: End-effector (Mobile platform); (h) 8: Base.

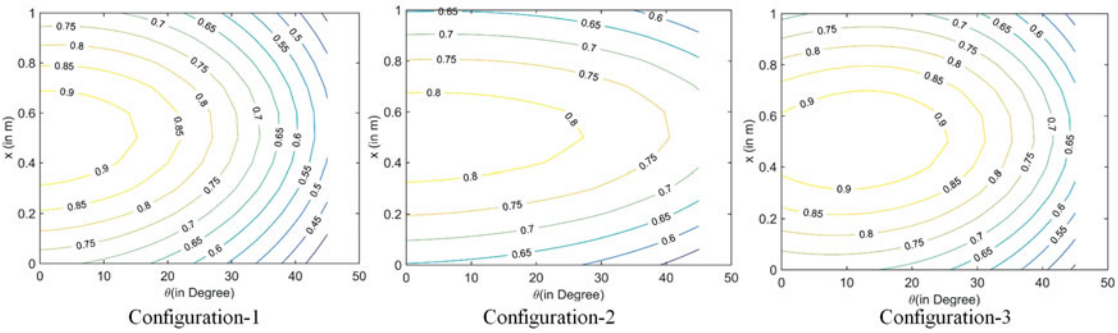

Fig. 9. Kinematic isotropy of the top-three U-shape fixed base manipulators associated with a square shape end-effector.

manipulator and its behaviour are not elaborated here. The design parameter values that provide better kinematic performances are only considered for the analysis. These values can be changed, and the results can be different from the present analysis. However, in this paper, it is left for the further study as a scope of future work.

https://doi.org/10.1017/S0263574718000267 Published online by Cambridge University Press

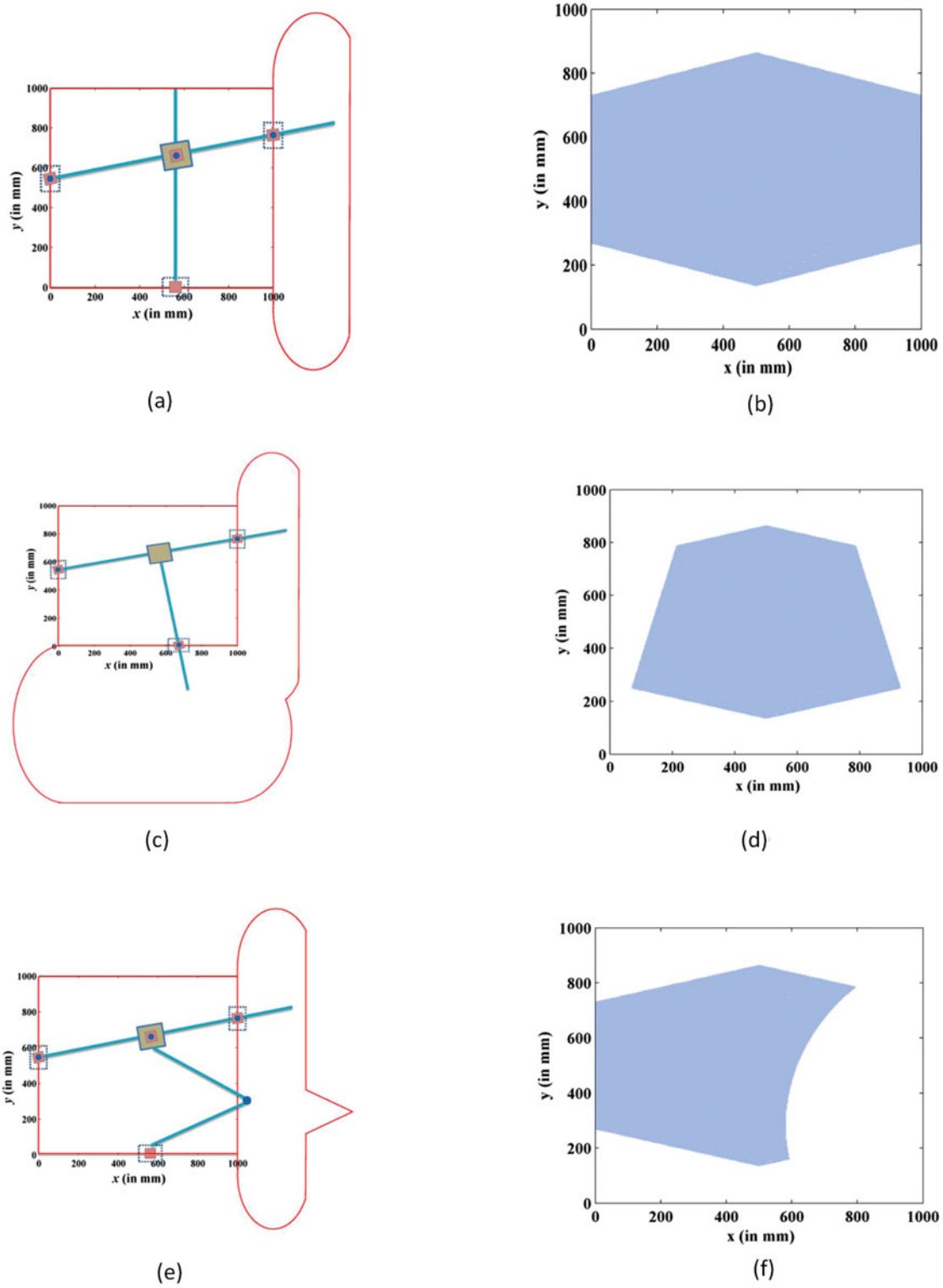

Fig. 10. Workspace and total area required at $\theta = [-15^\circ, +15^\circ]$ orientation angle. (a) Configuration-1 (total space required). (b) Configuration-1 (workspace). (c) Configuration-2 (total space required). (d) Configuration-2 (workspace). (e) Configuration-3 (total space required). (f) Configuration-3 (workspace).

https://doi.org/10.1017/S0263574718000267 Published online by Cambridge University Press

Table IX. Simulation parameters of the top-three manipulators for the analysis of dynamic performance.

Simulation parameters	Configuration-1	Configuration-2	Configuration-3
	Aspect ratio 0.5 (500 mm/1000 mm)		
r_1 (mm)	50–450	50–950	50–950
r_2 (mm)	50–450	50–950	50–950
r_3 (mm)	50–450	50–950	50–950
s (mm)		500	
	Aspect ratio 2 (1000 mm/500 mm)		
r_1 (mm)	50–950	50–450	50–450
r_2 (mm)	50–950	50–450	50–450
r_3 (mm)	50–950	50–450	50–450
s (mm)		1000	
	Aspect ratio 1 (1000 mm/1000 mm)		
r_1 (mm)	50–950	50–950	50–950
r_2 (mm)	50–950	50–950	50–950
r_3 (mm)	50–950	50–950	50–950
s (mm)		1000	
	Common parameters for all mentioned aspect ratios		
m (mass kg)	0.5	0.5	0.5
l_0(mm)	1000	–	–
l_1(mm)	1200	1000	400
l_2 (mm)	–	800	700
l_3(mm)	–	800	1200

- It is observed from the above analyses that configuration-1 and configuration-2 have improved, and favourable kinematic design aspects as shown in Figs. 3–5 are given in Tables V and X.

3. Energy Requirements and Dynamic Driving Performance

To identify the best manipulator among top-three PPMs, a comparative study of top-three best U-shape fixed base manipulator configurations based on their dynamic performance measures is investigated and discussed in this section. The size of the fixed platform or aspect ratio (width/height) can be varied for various working conditions to understand its design parameters and optimal design aspects, which are dependent on the fixed platform structure. Different aspect ratios (fixed platform size) are considered for the comparative analyses of energy requirements and dynamic driving performances for the top-three configurations. This section presents a comparative study on energy requirement and dynamic performance measure of the top-three manipulators with different aspect ratios (width/height), such as 0.5 (500 mm/1000 mm), 1 (1000 mm/1000 mm) and 2 (1000 mm/500 mm). This investigation reveals the information for the better selection of actuators, actuators capability and energy requirements of the manipulators, which are directly related to the efficiency and cost of the system. The analysis is performed numerically through the help of virtual prototypes based on the Adams/View multi-body software, and the geometric details of these manipulators are given in Table IX. For the dynamic analysis, a common circular trajectory tracking task is considered for these three different aspect ratios as mentioned earlier and given as follows:

$$x = 500 + 50\sin(0.12t), \text{ in mm} \tag{6}$$

$$y = 500 + 50\cos(0.12t), \text{ in mm} \tag{7}$$

$$\theta = 10^{\circ} \tag{8}$$

where t is the simulation time.

The total energy requirement of the manipulator configuration is given as follows:

$$E = \frac{1}{2}\sum_{i=1}^{n}\left(m_i\dot{x}_i^2 + m_i\dot{y}_i^2 + I\dot{\theta}^2\right) + m_i g y_i \tag{9}$$

https://doi.org/10.1017/S0263574718000267 Published online by Cambridge University Press

where E is the total energy required to accomplish the desired task. Also, m_i, I (i = 1 to n) are the active slider masses, passive prismatic joint masses, passive link masses, mobile platform mass and inertia, respectively. $\dot{x}_i$, $\dot{y}_i$, $\dot{\theta}$ (i = 1 to n) are the velocities of the mobile platform, active slider blocks and passive prismatic joints, respectively. Similarly, x_i, y_i (i = 1 to n) are the locations of the masses and inertias of the mobile platform, active slider blocks and passive prismatic joints, respectively. g is the acceleration due to gravity. The dynamic models of these manipulators are created in the MSC Adams/View and the desired circular motion is provided at the end-effector as given in relations from (6) to (8) for the different aspect ratios. The results of the multi-body dynamic analysis using the MSC Adams software are presented in the form of norm of energy requirements. The analysis of energy requirement for two different load conditions, namely no load (0 N) and full load (100 N) associated with the three different aspect ratios, is organised, and their obtained results are presented in Fig. 11(a)–(f). The detailed simulation results in terms of maximum, minimum and mean numerical values of the energy requirements of the top-three manipulators associated with three different aspect ratios are presented in Table X.

Figure 11(a)–(f) shows the dynamic performances of the top-three manipulators in terms of the energy requirements for three different aspect ratios and two loading conditions. From the results, it is found that the energy requirements for the aspect ratios 1 (1000 mm/1000 mm) and 2 (1000 mm/500 mm) are approximately the same for configuration-1 and configuration-2. It is also observed that the top-two manipulators (configuration-1 and configuration-2) have the same energy requirement as the aspect ratio increases (when aspect ratio increased with the variation of height of the fixed platform) from 1 and lower in the case of lower (when the aspect ratio increased with the variation of width of the fixed platform) aspect ratio. It is depicted from Table X that configuration-3 has the higher energy requirement when the aspect ratio of the fixed platform is 1 due to its structural arrangement. The results show that a high amount of energy is required to run the manipulator when the manipulator is operating at a higher load. The concluding remark observed from this Fig. 11 is that the energy requirement for configuration-1 is higher compared to other configurations. From the results and Table X, it is found that the minimum, maximum and mean numerical values of the energy requirement of configuration-2 are smaller compared to the other configurations due to the simplicity in its structure and the absence of any link interferences of within the workspace. Therefore, it can be concluded that the configuration-2 has the ability to perform any planar complex trajectory operation with the minimum input requirements within its workspace. Therefore, it will reduce the overall operation cost and improve the efficiency of the manipulator.

The top-three manipulator configurations, namely configuration-1, configuration-2 and configuration-3 have their own advantages and applications. The dynamic characteristics of top these configurations are important to reveal the specific applications of these manipulator configurations. The dynamic performance measure is a performance measure, which evaluates the force/torque margin of the joint forces/torques and obtained as[21,23,30]

$$p = \sqrt{\frac{1}{n}\sum_{i=1}^{n}\left(\frac{\tau_{\mathbf{i}}}{\boldsymbol{\tau}_{i\mathrm{Max}}}\right)^2} \tag{10}$$

where n is the number of actuated joints, $\tau_{\mathbf{i}}$ is the force/torques of joint i during the tracking a desired trajectory of the end-effector, and $\tau_{i\mathrm{Max}}$ is the maximum force/torque for joint i. The driving performance of the above-mentioned three PPMs becomes better in the case of lower dynamic performance index p.[33] In order to determine the driving torques and compare the dynamic performance measure of the three manipulators, the same values used for the energy requirement analysis are considered for the analysis. Table XI shows the simulation parameters of these configurations for the dynamic performance index (force/toque margin) analysis. This analysis is performed for both horizontal and vertical planar cases in order to understand the effect of gravity. Three different aspect ratios are selected for the analysis to show the dynamic driving performance of the manipulator configurations, and their simulation parameters are given in Table XI. The comparative dynamic driving performance index analysis is elaborated as shown in Fig. 12(a)–(f) and Table X. A few of the points are observed from the analyses and given as follows:

- It is found from the analysis that the dynamic driving performance for aspect ratios 1 and 2 is approximately the same for configuration-1 and configuration-2. The top-two manipulators

https://doi.org/10.1017/S0263574718000267 Published online by Cambridge University Press

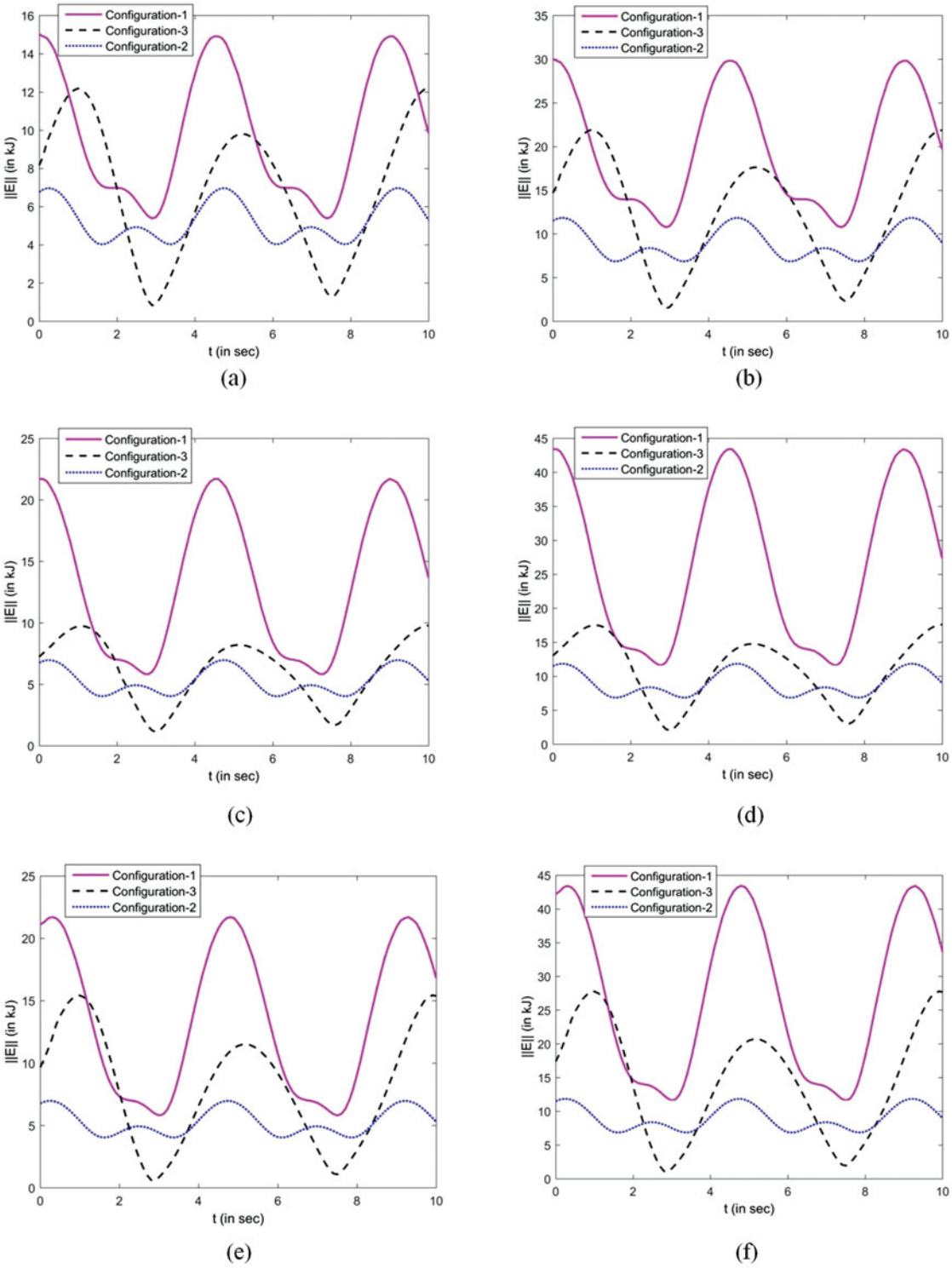

Fig. 11. Energy requirements of the top-three manipulator configurations (ADAMS simulation). (a) Aspect ratio (0.5) and no load (b) aspect ratio (0.5) and 100N load (c) Aspect ratio (2) and no load (d) Aspect ratio (0.5) and 100N load (e) Aspect ratio (1) and no load (f) Aspect ratio (0.5) 100N load.

(configuration-1 and configuration-2) show the same dynamic driving performance as the aspect ratio increases from 1 and lower in the case of lower aspect ratios.

- It is depicted from Table X that configuration-3 requires less amount of driving forces to follow the desired trajectory when the aspect ratio is 1. From Fig. 12 and Table X, it is found that the dynamic driving performance of the configuration-1 is lower and favourable than other configurations when

https://doi.org/10.1017/S0263574718000267 Published online by Cambridge University Press

Table X. Kinematic and dynamic performance measures comparison.

Comparative chart for kinematic isotropy of the top-three U-shape fixed base manipulators with two different end-effector connections to the legs									
End-effector connection to the legs (two different shapes)	Configuration-1 (PPR-PRP-PRP)			Configuration-2 (PRP-PRP-PRP)			Configuration-3 (PRR-PRP-PRP)		
	Max.	Min.	Mean	Max.	Min.	Mean	Max.	Min.	Mean
Equilateral triangle	0.94	0.35	0.71	0.82	0.51	0.71	0.94	0.43	0.75
Square	0.94	0.37	0.72	0.82	0.51	0.71	0.94	0.44	0.77
Energy requirement and dynamic performance measures (MSC ADAMS simulation)									
	Configuration-1			Configuration-2			Configuration-3		
Aspect ratio (W/H)	Max.	Min.	Mean	Max.	Min.	Mean	Max.	Min.	Mean
Energy consumption at no load (0 N) condition [‖E‖, kJ]									
0.5 (500 mm/1000 mm)	15.001	5.382	9.947	6.972	4.025	5.279	12.181	0.830	6.912
1 (1000 mm/1000 mm)	21.701	5.800	13.565	6.972	4.025	5.279	15.430	0.589	8.046
2 (1000 mm/500 mm)	21.702	5.809	13.400	6.972	4.025	5.279	9.785	1.125	6.094
Energy consumption at 100 N load condition [‖E‖, kJ]									
0.5 (500 mm/1000 mm)	30.003	10.763	19.894	11.853	6.843	8.974	21.926	1.493	12.442
1 (1000 mm/1000 mm)	43.403	11.600	27.131	11.853	6.843	8.974	27.774	1.061	14.482
2 (1000 mm/500 mm)	43.405	11.619	26.800	11.853	6.843	8.974	17.613	2.025	10.969
Dynamic driving performance measures (horizontal)									
0.5 (500 mm/1000 mm)	0.936	0.378	0.647	0.943	0.496	0.709	0.980	0.237	0.486
1 (1000 mm/1000 mm)	0.935	0.374	0.648	0.785	0.646	0.710	0.906	0.386	0.685
2 (1000 mm/500 mm)	0.935	0.374	0.648	0.830	0.587	0.711	0.954	0.371	0.660
Dynamic driving performance measures (vertical)									
0.5 (500 mm/1000 mm)	0.937	0.848	0.884	0.877	0.773	0.880	0.938	0.772	0.841
1 (1000 mm/1000 mm)	0.963	0.915	0.938	0.910	0.864	0.879	0.995	0.769	0.826
2 (1000 mm/500 mm)	0.963	0.915	0.938	0.901	0.876	0.884	0.976	0.744	0.821

the manipulator configurations are placed horizontally (without gravity). However, in the case of vertical arrangement of the manipulator, dynamic driving performance value of configuration-1 is high but not the best while compared with other configurations.

- From the results and Table X, it is found that the minimum, maximum and mean values of the dynamic driving performances of configuration-1 (horizontally case) and configuration-3 (vertical case) have favourable dynamic driving design aspects compared to the other configurations. Furthermore, the driving performances of the selected configurations are better when the gravitational effects are ignored. It can be noted that configuration-1 and configuration-3 have smaller values of mean of p such as (0.647, 0.648 and 0.648) and (0.841, 0.826 and 0.821) for three

https://doi.org/10.1017/S0263574718000267 Published online by Cambridge University Press

Table XI. Simulation parameters of the top-three manipulator configurations for the dynamic performance measure (force/torque margin).

Simulation parameters	Configuration-1	Configuration-2	Configuration-3
Aspect ratio 0.5 (500 mm/1000 mm)			
r_1 (mm)	50–450	50–950	50–950
r_2 (mm)	50–450	50–950	50–950
r_3 (mm)	50–450	50–950	50–950
s (mm)		500	
Aspect ratio 2 (1000 mm/500 mm)			
r_1 (mm)	50–950	50–450	50–450
r_2 (mm)	50–950	50–450	50–450
r_3 (mm)	50–950	50–450	50–450
s (mm)		1000	
Aspect ratio 1 (1000 mm/1000 mm)			
r_1 (mm)	50–950	50–950	50–950
r_2 (mm)	50–950	50–950	50–950
r_3 (mm)	50–950	50–950	50–950
s (mm)		1000	
Common parameters for all mentioned aspect ratio			
Mass of the end-effector, m_p (kg)	0.5	0.5	0.5
m_1, m_2, m_3, m_{s1}, m_{s2}, m_{s3}	0.5	0.5	0.5
l_0(mm)	1000	–	–
l_1 (mm)	1200	1000	400
l_2 (mm)	–	800	700
l_3 (mm)	–	800	1200

different aspect ratios of 0.5, 1 and 2, respectively. Therefore, configuration-1 and configuration-3 have the best driving performances compared to the others.

It is also observed from the analysis of dynamic performance measures with the consideration of gravitational effect that configuration-1 and configuration-2 have the lower maximum value of p, moderate minimum value of p and moderate mean value of p, respectively. Therefore, in some regions of the given workspace, configurations 1 and 2 have better driving performances compared to configuration-3.

4. Prototype Development and Experiments

Based on the comparative kinematic performance analyses of the U-shape fixed base manipulator configurations, it is observed that configuration-1, configuration-2 and configuration-3 have better performance measures compared to others. This section presents the experimental arrangements of these top-three manipulators to show the best manipulator among them on the basis of their energy requirements in the real time. Experiments have been conducted on an in-house fabricated reconfigurable/modular U-shape fixed base PPM. The proposed modular (reconfigurable) platform consists of a fixed platform in the shape of U having three prismatic joint actuators, whereas other structural arrangements (links, joints and end-effector) of each manipulator can be mounted as per kinematic arrangement, namely PPR-PRP-PRP, PRP-PRP-PRP and PRR-PRP-PRP for configuration-1, configuration-2 and configuration-3, respectively. Further, these experimental results are compared with the simulation results and validated their results. The entire dimension, size, weight and other parameters of the link, actuators, end-effector, base, etc. of the manipulators are considered the same for the simulation and the experimental setup. Details of the parameters of the simulation and the experimental setup are depicted in Table XII.

4.1. Development of the prototype of the top-three manipulators

The conceptual designs of the top-three configurations in the form of solid model are presented in Figs. 6–8. As discussed in the earlier section, the top-three U-shape fixed base configurations have three kinematic legs/chains as shown in Figs. 6–8, where the active prismatic actuators (joints) are made of

https://doi.org/10.1017/S0263574718000267 Published online by Cambridge University Press

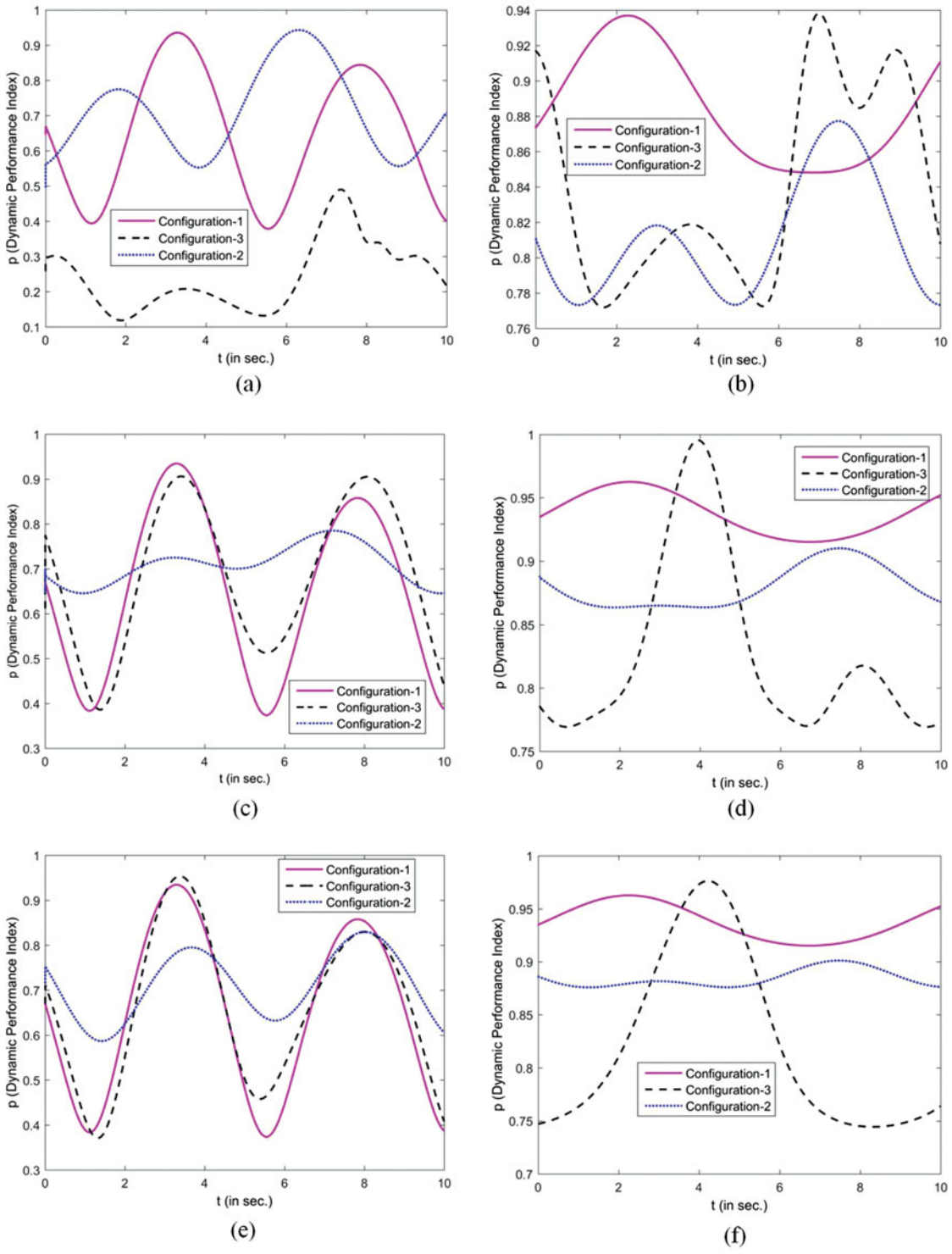

Fig. 12. Dynamic performance measures of the top-three U-shape fixed base configurations. (a) Horizontal (aspect ratio 0.5). (b) Vertical (aspect ratio 0.5). (c) Horizontal (aspect ratio 1). (d) Vertical (aspect ratio 1). (e) Horizontal (aspect ratio 2). (f) Vertical (aspect ratio 2).

screw joints along with the slider blocks (attached to the ball screws) act as prismatic joints. Electric motors are coupled with these linear ball screws with flexible couplings. Linear potentiometers (for displacement measurements) are connected to the block 6 to determine the position of the slider block 6.

https://doi.org/10.1017/S0263574718000267 Published online by Cambridge University Press

Table XII. Simulation and experimental setup parameters of the top-three manipulators.

Parameters	Configuration-1	Configuration-2	Configuration-3
	Aspect ratio 1 (500 mm/500 mm)		
r_1 (mm)	50–450	50–450	50–450
r_2 (mm)	50–450	50–450	50–450
r_3 (mm)	50–450	50–450	50–450
s (mm)		500	
	Common parameters		
Mass, m_p (kg)	0.250	0.250	0.250
m_1, m_2, m_3 (kg)	2	2	2
m_{s1} (kg)	2	1.25	0.250
m_{s2} (kg)	1	1	0.250
m_{s3}(kg)	1	1	2
l_0 (mm)	700	–	–
l_1 (mm)	700	550	350
l_2 (mm)	–	350	360
l_3 (mm)	–	350	700

In the case of configuration-1, the first linear ball screw 3 and the guide rail 5 situated in the x-axis are connected with the slider block 6, which in turn is connected with a passive link 4. A slider block moves on passive link 4 and acting like a passive prismatic joint. The slider block is connected with the end-effector (block 7) through a revolute joint (used a bearing and a pin). Similarly, the slider block 6 mounted on the second and third linear ball screws situated in the y-direction is connected with ball screw 3 and guide rail 5 along with a passive link 4 as shown in Fig. 6(b).

This passive link 4 is connected with block 6 through revolute joints. This link 4 is also connected to a moving platform 7, which slides on the passive link 4. All these links are situated in the xy-plane. In total, configuration-1 has eight rigid links that include the fixed and mobile platforms. It has nine single DOF joints that include six prismatic and three revolute joints. Therefore, based on Gruebler's mobility criterion, configuration-1 has 3-DOF.

In the case of configuration-2, the first linear ball screw 3 and the guide rail 5 situated in the x-axis are connected with the slider block 6, which is connected with a passive link 4 through a pin or revolute joint. One end of the passive link 4 is connected (fixed) with the end-effector (block 7). Similarly, slider block 6 situated in the y-direction is connected with a passive link 4 through revolute joints. This link 4 is also connected to a moving platform 7, which slides on the passive link 4 as shown in Fig. 7(b).

In the case of configuration-3, the first linear ball screw 3 and the guide rail 5 situated in x-axis are connected with the slider block 6. This block 6 is fixed with a first passive link 4 at a certain angle. One end of the first passive link 4 is connected with the second passive link 4 through a pin/rotary joint. Another end of the second passive link 4 is connected with the end-effector (block 7) via a pin or revolute joint. Similarly, the slider block 6 mounted on the second and third linear ball screws situated in the y-direction is connected with a passive link 4, and this passive link 4 is connected with the block 6 through a revolute joint. This link 4 is also connected to a moving platform 7, which slides on the passive link 4 as shown in Fig. 8(b).

4.2. Description of the experimental setup

To demonstrate the energy requirement of the top-three manipulators, the comparative dynamic performance analysis is performed by running real-time experiments and presented in Figs. 13–15. The same prototype models fabricated in real time are designed using solid model software, and their detailed descriptions about structure, joints and links are given in the previous subsections.

The MATLAB/SIMULINK software package is used for programming the controller, and Arduino Mega 2560 microcontroller board is used for feedback and hardware communication, as shown in Fig. 16. The Arduino board, which is having a clock speed of 16 MHz, is connected with a computer through a universal serial bus (USB) connection. It consists of two main interface modules: an analogue input module and a digital input output module. There are three DC motors connected to the ball screw joints via servo-flex shaft couplers; these DC motors are operated at 24 V having a maximum torque

https://doi.org/10.1017/S0263574718000267 Published online by Cambridge University Press

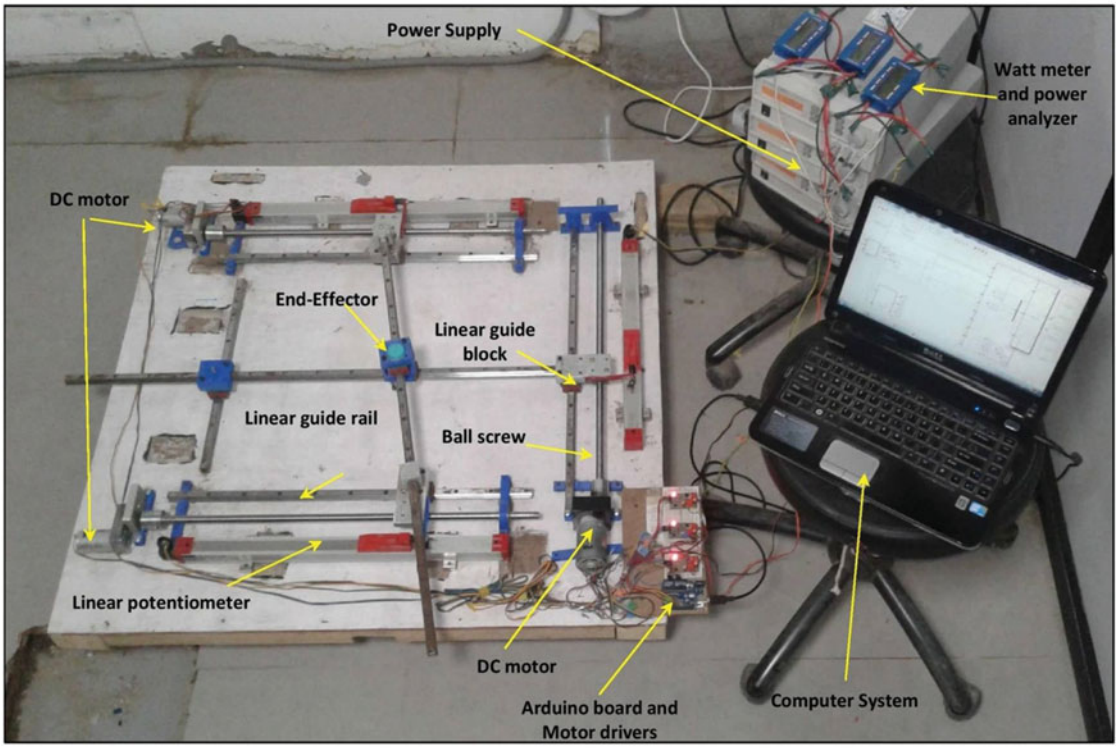

Fig. 13. PPR-PRP-PRP (configuration-1) manipulator experimental setup.

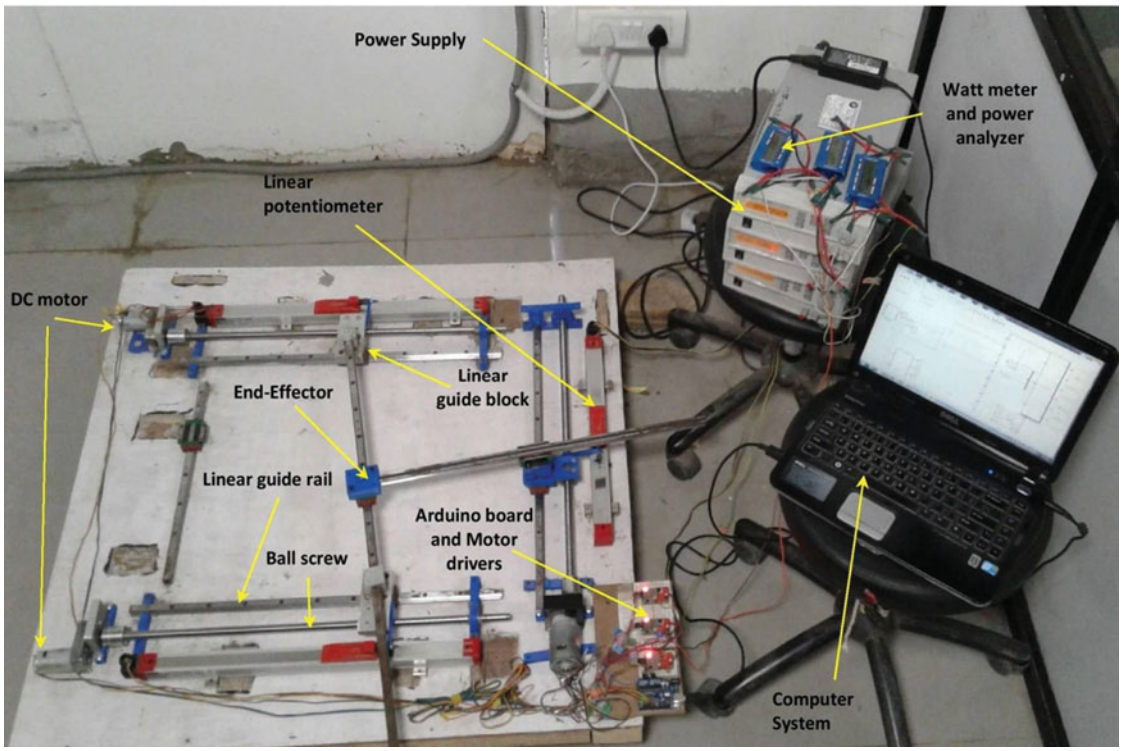

Fig. 14. PRP-PRP-PRP (configuration-2) manipulator experimental setup.

https://doi.org/10.1017/S0263574718000267 Published online by Cambridge University Press

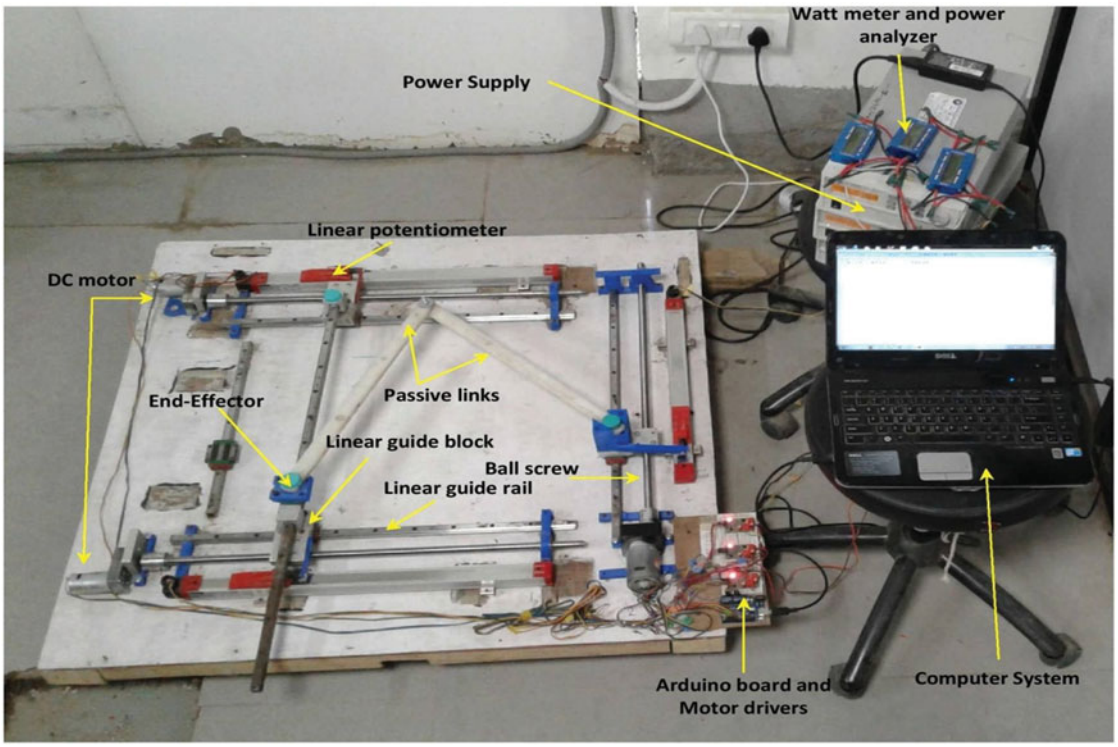

Fig. 15. PRR-PRP-PRP (configuration-3) manipulator experimental setup.

of 0.58 N m and max rpm of 1000. To control the DC motors, motor drivers with variable voltage control through PWM are installed, and to measure the joint displacements (positions) of the active prismatic joints, the DAQ system, which is equipped with linear potentiometers, is used as shown in Figs. 13–15. The linear potentiometers are having a stroke of 450 mm and a resolution of 0.1 mm. The energy requirement of the manipulators is obtained experimentally with the help of a DC watt meter and a power analyser. These manipulators (see Figs. 13–15) have a maximum workspace of 450 mm × 450 mm.

4.3. Experimental and simulation results and their comparison

To elaborate the energy requirement of the top-three configurations, experiments are performed on the fabricated prototypes and compared with the simulation results. All the parameters, dimensions and other necessary conditions are chosen the same for both simulation and experimental analyses, as shown in Table XII. Two different end-effector load conditions are considered for the energy requirement analysis, namely 0 N and 50 N. Task space variables chosen for the energy requirement for top-three manipulators are the same for the numerical simulations and experiments and given as follows:

Aspect ratio 1 (500 mm/500 mm)

$$x = 200 + 50\sin(0.1t), \text{ in mm} \tag{11}$$

$$y = 200 + 50\cos(0.1t), \text{ in mm} \tag{12}$$

$$\theta = 10^{\circ} \tag{13}$$

where t = 70 s is the total simulation time with a time step of 0.1 s.

The algorithm and process used for the energy requirement analysis (simulation as well as experiments) for these top-three configurations are presented in Figs. 16 and 17, respectively. The numerical results (simulation) of the top-three configurations for energy requirements are depicted in Fig. 18 and Table XIII. The concluding remark observed from Fig. 18 and Table XIII is that the energy requirement for configuration-1 is higher compared to the other top-two manipulators due

https://doi.org/10.1017/S0263574718000267 Published online by Cambridge University Press

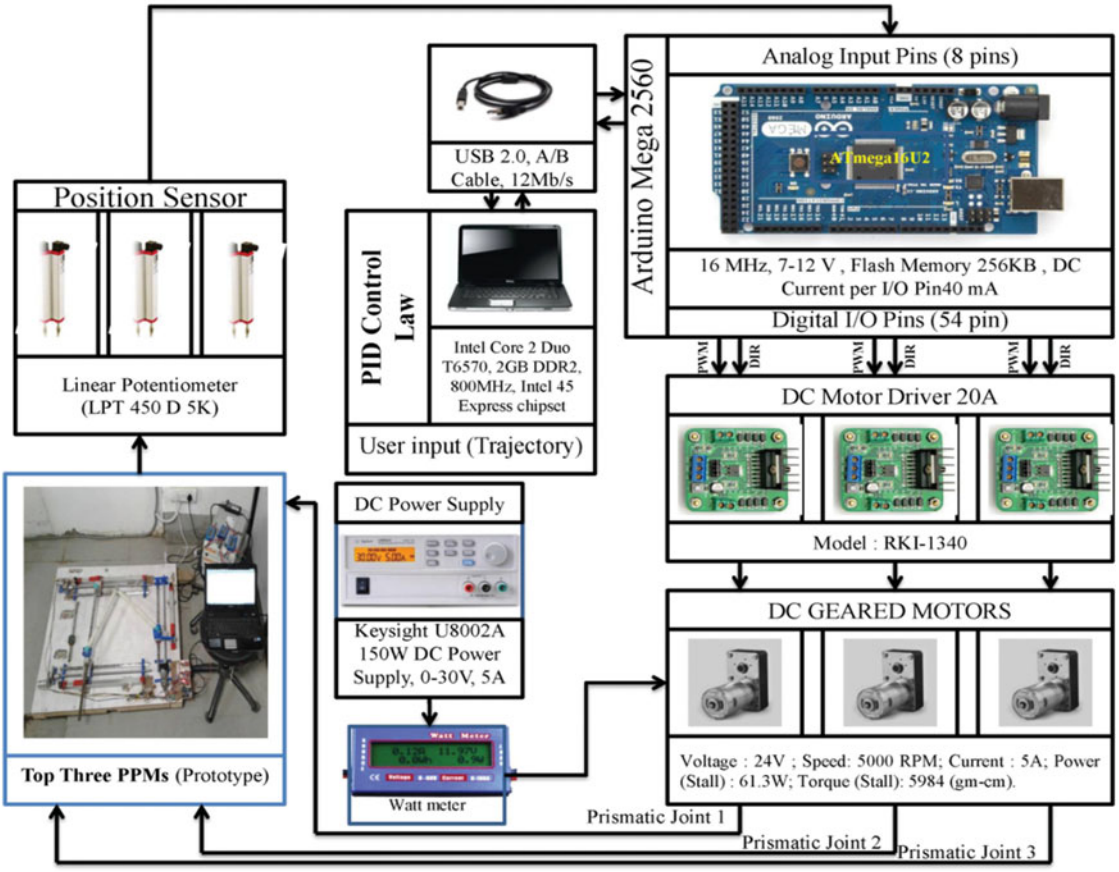

Fig. 16. Real-time architecture of the proposed experimental setup.

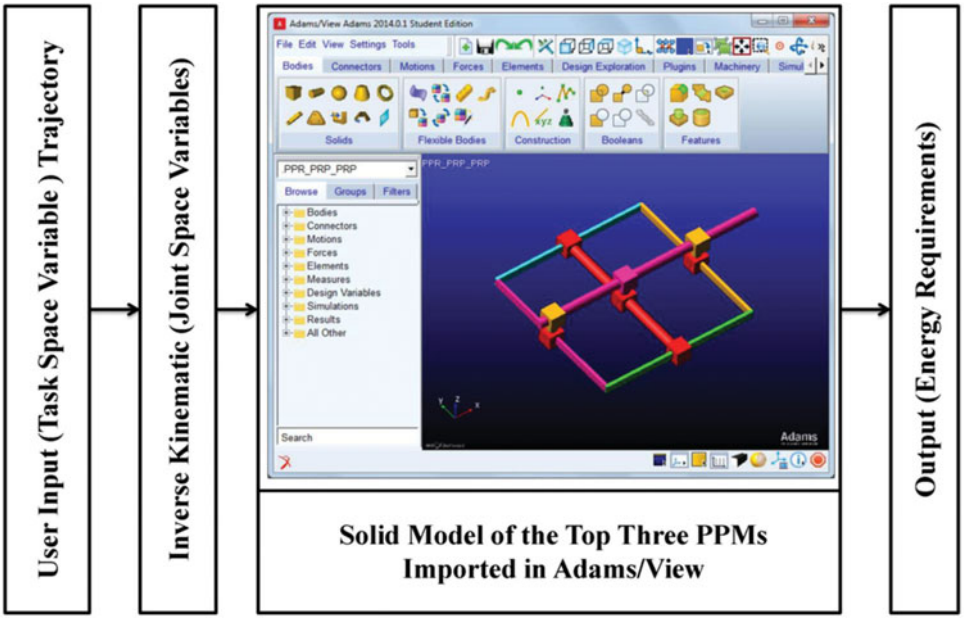

Fig. 17. Virtual prototype model of the proposed system in MSC Adams for simulations.

https://doi.org/10.1017/S0263574718000267 Published online by Cambridge University Press

Table XIII. Energy consumption of the top-three manipulators with aspect ratio 1 and a base size of 500 mm × 500 mm (simulation results).

Manipulator		Energy consumption (simulation results), ‖E‖ (kJ)		
		Max.	Min.	Mean
Configuration-1 PPR-PRP-PRP	At 0 N (no) load	2.6	0.999	1.704
	At 50 N load	5.022	1.997	3.408
Configuration-2 PRP-PRP-PRP	At 0 N (no) load	1.335	0.771	0.982
	At 50 N load	2.270	1.310	1.669
Configuration-3 PRR-PRP-PRP	At 0 N (no) load	1.954	0.806	1.189
	At 50 N load	2.876	1.532	1.982

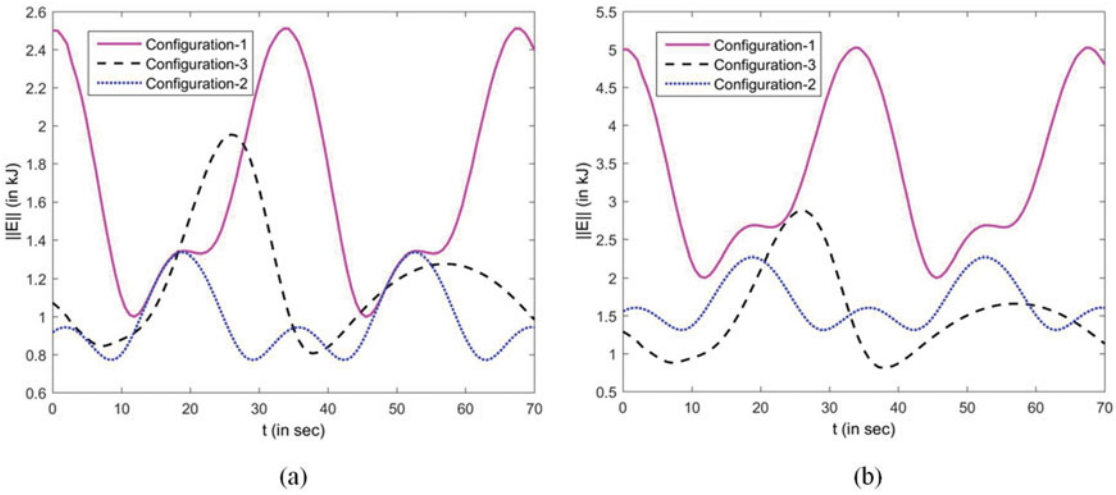

Fig. 18. Energy requirement of the top-three manipulators for two different end-effector loading conditions (aspect ratio 1, base size 500 mm/500 mm (simulation results)). (a) Energy requirement at 0 N. (b) Energy requirement at 50 N.

to its high amount of force requirements to push or pull the x-directional kinematic chain (PPR). Force requirement of the first leg of configuration-1 is high because of first active joint P of the PPR is required to push/pull and can be improved by providing a slight design modification in its kinematic arrangement. From the results and Table XIII, it is found that the energy requirement of the configuration-2 is low compared to the other configurations. Therefore, it can be concluded that configuration-3 has the ability to perform any planar complex trajectory operation with minimum input requirements within its workspace.

To validate the energy requirements of the top-three configurations, experiments are carried out for the same task-space trajectory, which is considered for the simulation analysis. The experimental results are compared with the simulation results. The block diagram of the experiments conducted is presented in Fig. 16 along with the step by step process for these top-three configurations. Figures 13–15 depicted the in-house fabricated prototypes of the top-three manipulator configurations on which the real-time experiments are performed.

Figure 16 presents the important components to perform the experiments, namely a user input block (trajectory) in association with conventional Proportional-integral-derivative (PID) control law, a power source, actuators, sensors, DC motor and drivers, a microcontroller block and a manipulator (robotic system). In the user input part, the desired manipulation task is defined (such as the type of operation, desired target task space positions, duration of the task and other particulars), and based on these information, the trajectory planner derives the time trajectories of the desired joint space position, velocity and acceleration vector (which is considered as a reference (input) vector for the PID control law) along with its inverse kinematics part. The robotic system (manipulators) part is composed of two sections, where the manipulator part represents the actual system. The sensor part measures

https://doi.org/10.1017/S0263574718000267 Published online by Cambridge University Press

Table XIV. Energy requirement of the in-house fabricated manipulator configurations.

Manipulator configuration aspect ratio = 1, (i.e., 500 mm/500 mm)		Experimental results					Simulation results
		$\|\|W_p\|\|$ (W)	$\|\|V_{min}\|\|$ (V)	$\|\|A_p\|\|$ (A)	$\|\|Ah\|\|$ (Ah)	$\|\|Wh\|\|$ (Wh)	$\|\|Wh\|\|$ (Wh)
Configuration-1	0 N (no) load	34.892	18.152	2.933	0.038	0.627	0.472
PPR-PRP-PRP	50 N load	79.37	19.32	5.97	0.058	1.349	0.946
Configuration-2	0 N (no) load	22.980	18.152	1.948	0.023	0.345	0.273
PRP-PRP-PRP	50 N load	37.17	18.75	3.87	0.043	0.648	0.464
Configuration-3	0 N (no) load	22.442	18.152	1.908	0.026	0.426	0.330
PRR-PRP-PRP	50 N load	36.85	18.152	3.34	0.051	0.739	0.550

Units: W (watt); Wh (watt-hour or 3600 joules); V (volt); A (ampere); Ah (ampere-hour).

the system states such as configuration space positions and velocities. The watt meter and power analyser are situated in between the DC power supply and DC motor to calculate the energy or power consumption of the system (manipulators), as shown in Fig. 16. The detailed process of experiments and the placement of the watt meter are presented in Fig. 16. The experiments are performed for two different end-effector loading conditions (0 N and 50 N), and their energy and power requirement values obtained from the experiments are presented in Table XIV. The watt meter gives the information about the voltage, current, charge, power and energy consumption about the system (actuators). The same information mentioned in the previous line is obtained from the experiments performed on the top-three manipulators, and the results are given in Table XIV. Energy requirement values obtained from the watt meter (experimental unit in W h) for mentioned manipulators are not the same unit as the values obtained from the numerical simulations (kJ). Therefore, for the comparative analysis, energy requirement numerical values obtained from the numerical simulation (in Table XIII) are converted to the same unit as obtained from the watt meter (in Table XIV), i.e., from kJ to Wh, and are presented in Table XIV.

It is found from the analysis that the energy requirement results obtained from experiments match closely with the numerical simulations (Adams/View virtual simulation) for both end-effector loading conditions, as shown in Table XIV. From Table XIV, it is observed that the energy requirement results obtained from both experiments and numerical simulations have a minor difference due to the presence of disturbances, friction and clearance in the component of in-house fabricated manipulators (prototype) as it has rotary and sliding joints, links elasticity and actuators' internal friction due to the reduction gear box.

It is also found from the results that configuration-2 has minimum requirement of energy to perform any planar complex trajectory operation compared to the other configurations, as shown in Table XIV.

5. Conclusions and Future Works

This paper has accomplished an in-depth research and performance investigations on a new family of U-shape fixed base manipulators to identify a better alternative to the conventional and existing manipulators. Specifically, the family of a three-legged PPM is starting with an active prismatic joint in each leg. The manipulator family's origin, configuration possibilities, kinematics and dynamics performances are discussed and analysed. The performance quantifiers in view of the system dynamics are investigated, and their comparative performance analyses are presented. Furthermore, to elaborate the energy requirements of the top-three best configurations, a set of real-time experiments are performed on the in-house fabricated prototypes. Further, the experimental results are confirmed with the virtual prototype simulations based on multi-body dynamics package, namely MSC ADAMS. A few valuable points are observed from the overall performance analyses and listed as follows:

1. It is observed from the performance investigations that configuration-1, configuration-2 and configuration-3 are better in terms of kinematic isotropy and structural arrangement.
2. From the results, it can be noted that configuration-1 has a larger workspace to total area required ratio, which is better than the other two configurations.

https://doi.org/10.1017/S0263574718000267 Published online by Cambridge University Press

3. The dynamic performance measures of the top-three configurations are significantly affected by the complex structure, placement of the actuators and presence of the number of links and joints.
4. Similarly, based on the dynamic driving performance analysis, it is also observed that the dynamic driving performance of the top-three manipulators is better in the absence of gravity effects.
5. From the overall results, it is found that the requirement of energy is less for configuration-2 under both no load (0 N) and full load (100 N) conditions due to its simple structure and absence of any interference of links within the workspace. But, in terms of the driving performance, this configuration is not as good compared to configuration-1 and configuration-3.
6. It is also observed from the aspect ratio (fixed platform size) analyses that the aspect ratio of the fixed platform affects the overall performance of the manipulators, and the dynamic performance is favourable for the squared-shaped fixed platform, i.e., the aspect ratio of the fixed platform is equal to 1.

It is perceived that the researchers can benefit from this performance analysis to select a proper PPM (as x, y and θ motion platform), which can be used for different macro- and micro-positioning/processing applications. The proposed work of this paper is primarily concerned about kinematic and dynamic performance measures of the U-shape fixed base manipulators. The accuracy and positioning error analysis of the robotic manipulators plays an important role to understand the behaviour of the manipulator system and reveals that how the clearance present in the joints (revolute and prismatic) affects the performance of the system. In this paper, the accuracy and the error (due to joint clearance and others) analyses are not considered either in simulations or experiments. Therefore, this work can be extended further in the direction of error analyses and experimental validation in the presence of joint clearances and other kinematic errors.

Acknowledgment

This work was supported by the Extramural Research scheme funded by the Council of Scientific and Industrial Research (CSIR), India (22(0698)/15/EMR-II/5767).

References

1. S. Briot and I. A. Bonev, "Are parallel robots more accurate than serial robots?," *Trans. Can. Soc. Mech. Eng.* **31**(4), 445–455 (2007).
2. J. P. Merlet, *Parallel Robots*, 2nd ed. (Springer, The Netherlands, 2006).
3. A. Joubair, M. Slamani and I. A. Bonev, "A novel XY-Theta precision table and a geometric procedure for its kinematic calibration," *Robot. Comput. Integr. Manuf.* **28**(1), 57–65 (2012).
4. I. A. Bonev, "Planar parallel mechanism and method," US Patent7707907 B2 (2010).
5. S. Staicu, "Inverse dynamics of the 3-PRR planar parallel robot," *Robot. Auton. Syst.* **57**(5), 556–563 (2009).
6. K. B. Choi, "Kinematic analysis and optimal design of 3-PPR planar parallel manipulator," *KSME Int. J.* **17**(4), 528–537 (2003).
7. S. Bai and S. Caro, "Design and Analysis of a 3-PPR Planar Robot with U-shape Base," *Proceedings of the ICAR International Conference on Advanced Robotics*, Munich, Germany (2009) pp. 1–6.
8. J. Wu, J. Wang, L. Wang and Z. You, "Performance comparison of three planar 3 DOF parallel manipulators with 4-RRR, 3-RRR and 2-RRR structures," *Mechatronics* **20**(4), 510–517 (2010).
9. J. P. Merlet, C. M. Gosselin and N. Mouly, "Workspaces of planar parallel manipulators," *Mech. Mach. Theory* **33**(1–2), 7–20 (1998).
10. A. Rezaei and A. Akbarzadeh, "Position and stiffness analysis of a new asymmetric 2PRR-PPR parallel CNC machine," *Adv. Robot.* **27**(2), 133–145 (2013).
11. G. Gogu, *Structural Synthesis of Parallel Robots, Part 1: Methodology*, 1st ed. (Springer, The Netherlands, 2008).
12. G. Gogu, *Structural Synthesis of Parallel Robots, Part 2: Translational Topologies with Two and Three Degrees of Freedom*, 1st ed. (Springer, The Netherlands, 2009)
13. G. Gogu, *Structural Synthesis of Parallel Robots, Part 3: Topologies with Planar Motion of the Moving Platform*, 1st ed. (Springer, The Netherlands, 2010).
14. G. Gogu, *Fully-Isotropic T3R1-Type Parallel Manipulators, on Advances in Robot Kinematics* (Springer, The Netherlands, 2004) pp. 265–272.
15. A. Yu, I. A. Bonev and P. Z. Murray, "Geometric approach to the accuracy analysis of a class of 3 DOF planar parallel robots," *Mech. Mach. Theory* **43**, 364–375 (2008).
16. V. H. Arakelian and M. R. Smith, "Design of planar 3 DOF 3-RRR reactionless parallel manipulators," *Mechatronics* **18**, 601–606 (2008).

17. S. Briot and I. A. Bonev, "Accuracy analysis of 3 DOF planar parallel robots," *Mech. Mach. Theory* **43**, 445–458 (2008).
18. S. Staicu, "Dynamics of a 3-RPR planar parallel robot," *UPB Sci. Bull. Ser. D*, **70**(3), 3–18 (2008).
19. S. Caro, N. Binaud and P. Wenger, "Sensitivity analysis of 3-RPR planar parallel manipulators," *J. Mech. Des.* **131**, 121005-1–13 (2009).
20. N. Binaud, S. Caro and P. Wenger, "Sensitivity comparison of planar parallel manipulators," *Mech. Mach. Theory* **45**(11), 1477–1490 (2010).
21. J. Wu, J. Wang and Z. You, "A comparison study on the dynamics of planar 3 DOF 4-RRR, 3-RRR and 2-RRR parallel manipulators," *Robot. Comput. Integr. Manuf.* **27**(1), 150–156 (2011).
22. G. Wu, S. Bai, J. A. Kepler and S. Caro, "Error modelling and experimental validation of a planar 3-PPR parallel manipulator with joint clearance," *J. Mech. Robot.* **4**, 041008-1–12 (2012).
23. J. Wu, T. Li, J. Wang and L. Wang, "Performance analysis and comparison of planar 3 DOF parallel manipulators with one and two additional branches," *J. Intell. Robot. Syst.* **72**, 73–82 (2013)
24. S. Staicu, "Power requirement comparison in the 3-RPR planar parallel robot dynamics," *Mech. Mach. Theory*, **44**, 1045–1057 (2009).
25. N. Binaud, S. Caro and P. Wenger, "Comparison of 3-RPR planar parallel manipulators with regard to their kinetostatic performance and sensitivity to geometric uncertainties," *Meccanica* **46**, 75–88 (2011).
26. O. Khatib, "Inertial properties in robotic manipulation: An object-level framework," *Int. J. Robot. Res.*, **14**, 19–36 (1995).
27. J. Wu, Y. Gao, B. Zhang and L. Wang, "Workspace and dynamic performance evaluation of the parallel manipulators in a spray-painting equipment," *Robot. Comput.-Integr. Manuf.* **44**, 199–207 (2017).
28. W. Liping, X. Huayang and G. Liwen, "Kinematics and inverse dynamics analysis for a novel 3-PUU parallel mechanism," *Robotica* **35**(10), 1–18 (2016).
29. D. Liang, Y. Song, T. Sun and G. Dong, "Optimum design of a novel redundantly actuated parallel manipulator with multiple actuation modes for high kinematic and dynamic performance," *Nonlinear Dyn*. **83**(1), 631–658 (2016).
30. J. Wu, J. Wang, T. Li and L. Wang, "Dynamic analysis of the 2 DOF planar parallel manipulator of a heavy-duty hybrid machine tool," *Int. J. Adv. Manuf. Technol.*, **34**, 413–420 (2007).
31. S. Patel and T. Sobh, "Manipulator performance measures: A comprehensive literature survey," *J. Intell. Robot. Syst.* **77**(3), 547–570 (2015).
32. Z. Yongjie and G. Feng, "Dynamic formulation and performance evaluation of the redundant parallel manipulator," *Robot. Comput. Integr. Manuf.* **25**, 770–781 (2009).
33. L. D. Keith, M. S. Eric and B. Claudio, "Robot manipulability," *IEEE Trans. Robot. Autom.* **11**(3), 462–468 (1994)
34. F. C. Park and R. W. Brockett, "Kinematic dexterity of robotic mechanisms," *Int. J. Robot. Res.* **13**(2), 1–15 (1994).
35. T. J. Graettinger and B. H. Krogh, "The acceleration radius: A global performance measure for robotic manipulators," *IEEE J. Robot. Autom.* **4**, 60–69 (1988).
36. Y. Singh, *Performance Investigations on Mechanical Design and Motion Control of Planar Parallel Manipulators*, *Ph.D. Thesis* (Indore, Indian Institute of Technology Indore, 2016).
37. S. Kucuk, "A dexterity comparison for 3 DOF planar parallel manipulators with two kinematic chains using genetic algorithms," *Mechatronics* **19**(6), 868–877 (2009).
38. J. O. Kim and P. K. Khosla, "Dexterity Measures for Design and Control of Manipulators," *Proceedings of the IEEE/RSJ International Workshop on Intelligent Robots and Systems*, Osaka, Japan (1991) pp. 758–763.
39. T. Yoshikawa, "Manipulability of robotic mechanisms," *Int. J. Robot. Res.* **4**(2), 3–9 (1985).
40. D. Kees and D. K. Pai, "Performance measures for robot manipulators: A unified approach," *Int. J. Robot. Res.* **15**(1), 92–111 (1996).
41. S. Kucuk and Z. Bingul, "Comparative study of performance indices for fundamental robot manipulators," *Robot. Auton. Syst.* **54**(7), 567–573 (2006).
42. Y. Singh and S. Mohan, "Kinematic Performance Analysis of a New 2PRP-PRR Planar Parallel Robotic Manipulator," *Proceedings of the 4th Joint International Conference on Multibody System Dynamics*, Montréal, Québec, Canada (2016).